HHS Public Access

Author manuscript

Nat Metab. Author manuscript; available in PMC 2022 March 20.

Published in final edited form as:

Nat Metab. 2021 September ; 3(9): 1259–1274. doi:10.1038/s42255-021-00450-3.

Heritable shifts in redox metabolites during mitochondrial quiescence reprogram progeny metabolism

Helin Hocaoglu[1,*], **Lei Wang**[1,*], **Mengye Yang**[1,*], **Sibiao Yue**[1], **Matthew Sieber**[1]

[1)]Department of Physiology, UT Southwestern Medical Center, 5323 Harry Hines Blvd, Dallas, TX. 75390

Abstract

Changes in maternal diet and metabolic defects in mothers can profoundly impact progeny health and disease. However, the biochemical mechanisms that induce the initial reprogramming events at the cellular level have remained largely unknown due to limitations in obtaining pure populations of quiescent oocytes. Here, we show that the precocious onset of Mitochondrial Respiratory Quiescence (MRQ) causes a reprogramming of progeny metabolic state. The premature onset of MRQ drives the lowering of Drosophila oocyte NAD+ levels. NAD+ depletion in the oocyte leads to reduced methionine cycle production of the methyl donor S-adenosylmethionine (SAM) in embryos and lower H3K27-me3 levels, resulting in enhanced levels of progeny intestinal lipid metabolism. In addition, we show that triggering cellular quiescence in mammalian cells and chemotherapy-resistant human cancer cell models induces cellular reprogramming events identical to those seen in Drosophila, suggesting a conserved metabolic mechanism in systems reliant on quiescent cells.

Introduction

Metabolic dysfunction is a key factor that greatly impacts lifespan and increases a person's risk for heart disease, neuropathy, and certain types of cancers [1-3]. While environmental factors and nutrition play an essential role in the incidence of metabolic diseases, many studies have suggested that maternal metabolism can profoundly impact progeny physiology, disease susceptibility, and overall lifespan. [4-7]. Previous studies in *C.elegans*, *Drosophila*,

Corresponding author and lead contact= matthew.sieber@utsouthwestern.edu.

*These authors contributed equally

Author contributions:

L.W., H.H., M.Y., S.Y., and M.S. designed and conducted the experiment described in this manuscript. L.W., H.H., and M.S. analyzed the data and wrote the manuscript.

Contact for Reagent and Resource Sharing

Further information and requests for resources and reagents should be directed to and will be fulfilled by the Lead Contact, Matthew Sieber (matthew.sieber@utsouthwestern.edu)

Conflict of interest

The authors in this manuscript have no conflicts of interest to report.

Data Sharing

RNA seq and ChIP data for figures 4 and 8 have been deposited under accession numbers: GSE145353, GSE175387 GSE175754, GSE175755, and GSE175756. Metabolomics data for InR-DN oocytes is provided in source data. All other data supporting these findings are available within this manuscript.

and mammals suggest that disruptions in parental metabolic state cause changes in germ cell chromatin status [8,9]. However, many of these studies infer changes in the oocyte by examining chromatin and small RNA changes in the progeny. During oogenesis, germ cells undergo a reprogramming of epigenetic state that resets the genome for embryonic development [10,11]. This germline reprogramming presents an obstacle for metabolism-induced changes in oocyte chromatin. Unlike sperm, progeny inherit a sophisticated stockpile of stored nutrients, metabolites, and mitochondria from the oocyte. Moreover, recent studies have shown metabolites such as NAD+, acetyl-CoA, and alpha-ketoglutarate can control gene expression through the activity of chromatin regulators [1213]. These studies support the idea that changes in metabolites in quiescent oocytes may function in the reprogramming of progeny metabolism. However, due to limitations in obtaining pure populations of *in vivo* quiescent cells, it remains unclear how metabolite levels in the oocyte impact progeny metabolic reprogramming in many model systems.

Previously we found that, as oocytes enter cellular quiescence, loss of insulin signaling causes the remodeling of the mitochondria and suppression of respiration in a process we have named Mitochondrial Respiratory Quiescence (MRQ)[14]. Consistent with the known role of insulin signaling in oocyte development[15-17] and nutrient-sensing, we have shown that MRQ is conserved in vertebrates and is triggered by suppression of Akt[14]. These studies provided us with tools to examine how nutrient stress alters cellular physiology in quiescent cells to determine how this may impact the reprogramming of progeny metabolism. Using Drosophila oogenesis as a model, we show that cells establish a unique state of redox metabolism as they enter MRQ. Here we use *Drosophila* and mammalian cell systems to define how dynamic shifts in redox metabolites during quiescence drive the reprogramming of progeny metabolism. Overall, these studies show that cellular quiescence provides a conserved physiological state that facilitates the reprogramming of progeny metabolism during reproduction and cancer recurrence.

Results

Previous studies have investigated the impact of maternal diet on progeny physiology and health by examining how parental metabolic stress alters chromatin status and small RNA levels in progeny [8]. However, these studies did not consider the quiescent nature of oocytes and how this shift in cellular physiology may impact the reprogramming of progeny metabolism. As a result, the molecular mechanisms driving progeny metabolic reprogramming remain unclear because the biochemical changes in quiescent oocytes are largely undefined. This deficiency is primarily due to limitations in obtaining sufficient amounts of *in vivo* quiescent oocytes to conduct these studies. Our lab exploits *Drosophila* oogenesis as a system to obtain large quantities of staged quiescent oocytes for in-depth biochemical characterization of these cells and gain a molecular understanding of their impact on offspring physiology. We combine these studies with mammalian and human cell systems to uncover the conserved biochemical pathways that underlie the reprogramming of progeny metabolism.

Germline metabolic stress reprograms progeny metabolism.

During *Drosophila*, oogenesis follicles progress through 14 distinct stages of development. Follicles grow up until stage 10 of oogenesis, at which time they begin the transition into quiescence, and by stage 14, the oocytes are completely quiescent. Our previous work showed that the premature suppression of insulin signaling induces MRQ during early germ cell development[14]. To examine the role of MRQ in the reprogramming of progeny metabolism, we disrupted germline insulin signaling either genetically, by expressing InR-DN [18] in germ cells using MTD-GAL4[19], or by feeding females an amino acid-deficient diet and crossing those females to wild-type males. We then collected progeny that was either MTD-GAL4/+ or UAS-InR-DN/+ and assayed the resulting adult progeny for changes in embryonic mitochondrial function and glucose and triglyceride metabolism (Fig 1 A and C). Suppressing germline insulin signaling by expressing an InR-DN in female germ cells causes elevated levels of mitochondrial activity in embryonic progeny compared to the progeny of MTD-GFP control females (Fig 1B). In addition, the adult progeny of InR-DN expressing oocytes display increased levels of glucose (Fig 1D), glycogen (Extended Data Fig 1A), trehalose (Extended Data Fig 1B), and triglycerides (Fig 1E), consistent with a life-long reprogramming of progeny energy metabolism. We confirmed these results by inhibiting the insulin effector TOR in germ cells (TOR-DN) [20] and observed similar changes in progeny metabolites (Fig 1D & E). Interestingly, the increased levels of glucose, glycogen, and triglyceride in progeny are replicated by feeding control mothers (*Oregon R*) an amino acid-deficient diet, suggesting the reprogramming of progeny metabolism by nutrient depletion observed in many species is mediated in part by alterations in germline insulin signaling (Fig 1F)(Extended Data Fig 1 C&G). This effect was not due to the genetic background given that feeding amino acid-deficient media to *canton S, yw, and Oregon* R flies induced similar reprogramming of glucose and triglyceride metabolism in progeny (Extended Data Fig 1 D&E). We observed no changes in sterol levels suggesting the reprogramming effect is limited to processes involving energy homeostasis (Extended Data Fig 1 F).

Interestingly, we found that the reprogrammed progeny from InR-DN expressing oocytes survive 2.5-times better under poor nutrient conditions than control progeny (Fig 1G). Reprogrammed progeny also display higher glucose levels under low nutrient conditions, and these phenotypes are suppressed by feeding a rich diet, suggesting that progeny metabolic reprogramming enhances survival in a poor nutrient environment (Fig 1H). While these reprogrammed progeny display an enhanced ability to develop under poor nutrient conditions, their altered metabolic program leads to a shortened lifespan (Fig 1I). These data indicate that progeny metabolic reprogramming causes physiological tradeoffs that support development to reproductive age in a poor nutrient environment at the expense of lifespan. Disrupting the insulin pathway transcriptional effector, *foxo*, however, had no impact on progeny metabolism consistent with our previous work that shows that MRQ is a *foxo* independent process (Extended Data Fig 1 H, I).

Premature MRQ remodels redox metabolism in mature oocytes.

To understand how altering MRQ could impact progeny reprogramming, we examined the metabolic changes that occur as oocytes transition from growth (stage 8) and enter

quiescence (stage 14). Consistent with our previous studies, we found that mitochondrial membrane potential is lost during stage 10 as follicles as developing follicles transition from growth to quiescence (Fig 2A). We have found that this loss of mitochondrial membrane potential is associated with a dramatic reduction in respiration that lasts through quiescence until embryonic growth resumes and mitochondrial activity is restored (Fig 2B). We observed a shift in redox metabolism during this transition that leads to a 3-fold increase in NAD^+/NADH ratio in mature oocytes (Fig 2C). Using metabolomics, we observed a shift in the pyruvate/lactate ratio (Fig 2E), the malate/aspartate ratio (Fig 2D), and a build-up of glycolytic intermediates (Fig 2G). We also documented a build-up of TCA cycle intermediates such as alpha-ketoglutarate, succinate, malate, and fumarate (Extended Data Fig 2C). These data suggest that a shift in NAD^+ redox metabolism is caused by a block in NAD^+ regeneration (by LDH and the malate/aspartate shuttle) as well as impaired NADH production (from glycolysis and the TCA cycle) (see the model in Fig 2F). This suppression of mitochondrial oxidative metabolism is also associated with increased stored glycogen and triglycerides (Extended Data Fig 2A and B). We hypothesized that establishing this unique state of NADH redox metabolism during MRQ plays a vital role in the reprogramming of progeny metabolism. Consistent with this idea, recent studies have shown that this unique reduced state is again altered during egg activation and early embryogenesis as a global shift in NAD/NADH and glutathione (GSSG/GSH) redox metabolism primes the embryo for growth [21,22].

Metabolites can function as heritable factors.

To examine the impact that the premature onset of MRQ has on the metabolic state of quiescent oocytes, we suppressed insulin signaling in germ cells. Compared to MTD-GFP control ovarioles, expressing InR-DN or TOR-DN in germ cells causes reduced mitochondrial membrane potential in early egg chambers and the premature onset of MRQ (Fig 3A). We confirmed these results by measuring mitochondrial oxidative metabolism in these ovarioles. We found that insulin inhibition causes lower respiration levels while culturing ovarioles with exogenous insulin increases mitochondrial respiration significantly (Extended Data Fig 3F). Interestingly, using LC/MS metabolomics, we found that the premature onset of MRQ causes a shift in the levels of 45 metabolites in InR-DN expressing oocytes (Extended Data Fig 3A), including a reduction in the levels of NAD^+, kynurenine (NAD^+ precursor), and cADP-ribose (a product made from NAD^+), as well as a build-up of nicotinic acid, a substrate for NAD^+ biosynthesis (Fig 3B). We observed a 60% reduction in NAD^+/NADH (Fig 3C) ratio and a 70% reduction in NAD^+/nicotinic acid ratio (Fig 3D) consistent with defective NAD^+ production via the Priess-Handler pathway (Extended Data Fig 3B). This data is consistent with the fact that *Drosophila* relies heavily on the Priess-Handler pathway because flies lack QAPRT, the enzyme that converts Q.A. to NAMN. We also observed reduced oxidized glutathione (GSSG) production from cysteine, and a lower GSSG/GSH ratio, further supporting the idea that redox metabolism is altered in reprogrammed oocytes (Fig 3B and E). We also observed reduced levels of short-chain acyl-carnitines and a build-up of purine intermediates (Extended Data Fig 3C-E). These data are consistent with the model that the premature onset of MRQ disrupts the unique balance of redox metabolites in quiescent oocytes that may induce the reprogramming of progeny metabolism.

In testing this model, we found that disrupting NADPH production maternally by inhibiting the pentose phosphate pathway during oogenesis leads to adult progeny that display similar reprogramming of glucose and triglyceride metabolism that we observed in progeny reprogrammed by precocious MRQ entry (Extended Data Fig 4A and B). When we examined the role of NAD^+ biosynthesis in progeny metabolic reprogramming, we found that feeding a maternal diet supplemented with nicotinamide mononucleotide (NMN) or a diet supplemented with nicotinamide riboside and nicotinic acid (N.A. and N.R.) rescues the reprogramming of glucose (Fig 3F) and triglyceride (Fig 3G) metabolism observed in progeny from InR-DN expressing oocytes (Extended Data Fig 4C). Moreover, we discovered that inhibiting the expression of the Preiss-handler pathway enzyme NAPRT maternally in germ cells using RNAi[23] is sufficient to reproduce the glucose and triglyceride metabolism phenotypes observed in the progeny of InR-DN expressing oocytes (Fig 3 H and I). Overall, these data show that the levels of a single metabolite, NAD^+, functions as a heritable factor that drives the reprogramming of progeny physiology and metabolism.

To gain a molecular understanding of the cause of this shift in NAD+, we examined gene expression in MTD-GFP and MTD-InR-DN expressing oocytes using mRNA sequencing. We found that 952 genes display differential expression by at least a log2 fold change greater than 1 (FDR<.05). Of these genes, 83% (790) were down-regulated in InR-DN expressing oocytes (Fig 4A and C). Gene Ontology analysis of these genes showed they are enriched for broad terms such as coiled-coiled, alternative splicing, phosphoprotein, and developmental protein (Extended data Fig 5B). These observations are consistent with the fact that the oocyte must store all of the transcripts required for late oogenesis and early embryogenesis until the zygotic genome activates. These maternally loaded genes include everything from genes encoding structural proteins (actin and alpha-tubulin), metabolic genes, to genes encoding the signaling pathway members (Notch and Ras Family GTPases). For example, we observed a subset of maternally loaded transcription factors that display decreased expression in InR-DN expressing oocytes (Extended Data Fig 5A). These data suggest that insulin inhibition triggers the early onset of quiescence and reduced maternal RNA storage.

We further examined this list of down-regulated genes to determine how redox metabolism is altered in oocytes upon InR-DN expression. Consistent with the widespread changes in mitochondrial metabolism and redox homeostasis in InR-DN expressing oocytes, we found that 129 of these genes overlap with a published list of *Drosophila* metabolism genes (Fig 4B) [2224]. Notably, 93 genes are involved with redox metabolism were down-regulated in this data set (Extended data tabl 1). These genes include processes such as NADH and glutathione metabolism (Fig 4D), mitochondrial metabolism (Fig 4F), and glycolysis/ gluconeogenesis (Extended data Fig 5J). Interestingly, a subset of these genes have known roles in the NAD/NADH balance in the cytosol or are components of pathways involved with NAD biosynthesis (NAAM, NAD synthase, and NADK) (Fig4 D and E). These data indicate that reduced NAD regeneration and impaired NAD biosynthesis drive the low levels of NAD and InR-DN expressing oocytes.

Interestingly, many of these genes are maternally loaded like MDH2 (Extended Data Fig 5E) (Extended data table 1). In conjunction with an altered redox state, these data show

that InR-DN expressing oocytes also display defective loading of mRNAs that promote redox homeostasis in the early embryo. Consistent with this idea, we examined the redox state of the embryonic progeny of InR-DN expressing oocytes using a transgenic cytosolic redox reporter (roGFP) in embryos at 4-6 hrs and 16-20 hrs of development. In line with our metabolomic and RNA sequencing results, we found that early embryonic progeny from InR-DN oocytes display a more reduced redox state relative to controls. However, this reduced state is corrected during late embryogenesis (Extended data Fig 5 C, D, F, G, H, I). Overall, these data are consistent with the model that the premature onset of MRQ in oocytes creates a reduced redox environment during early embryogenesis that induces progeny reprogramming.

Altered intestinal metabolism underlies metabolic reprogramming.

To define the metabolic changes that drive the reprogramming of progeny metabolism, we conducted RNA-sequencing on the 16hr embryonic progeny of MTD-GFP and InR-DN expressing oocytes. We identified 668 differentially expressed genes in reprogrammed embryonic progeny (fold change cutoff 1.5 and FDR <.05). Among these genes, the majority were up-regulated (343 up and 325 down), and fold-changes associated with the up-regulated genes were more dramatic than downregulated. We found that 26 up-regulated genes encode proteins involved with calcium/cAMP signaling consistent with the elevation of mitochondrial activity in reprogrammed progeny (Fig 4H). In addition, 39% (136) of the up-regulated genes display enriched expression in the adult intestine when examined for overlap with a recently published list of intestinally expressed genes (Fig 4G). These include genes involved with numerous aspects of intestinal metabolism, including digestion (*CG12374, Jon25bi, Jon99Ci, Jon74E, Jon65Avi, alpha-trypsin, gamma-trypsin*), lipid homeostasis (*magro, CG6295, CG17192, CG9394, GLaz, CG8834*), carbohydrate metabolism (*Mal-A6, Amy-d, Amy-p, Mal-A1, CG6484, CG4607*) and nutrient transport (*CG32053, CG30272, CG8083, CG15096, Ocrt, CG2187*). In fact when we examine the top 5 gene ontology terms enriched in the list include Proteolysis/protease/zymogen(FDR< 5.3x10^−8), calcium (FDR= 3.02x10^−4), lipid metabolism (FDR= 8.9x10^−4), sugar transporter (FDR= 2.9x10^−4), and substrate-specific transport activity (FDR= 5.4x1^−4). Using, transcriptomic data from the modENCODE project we examined the tissue and developmental expression of these genes [25]. We found that many of these genes have precise expression in the intestine (Fig 4L) (Extended data Fig 6D) and display little to no expression in the embryo but show high expression levels in the larval and adult intestine (Fig 4J,I), (Extended Data Fig 6 C, Dand F) [25]. However, we observed high expression levels for these genes during mid-embryogenesis (Fig 4 G,J) (Extended Data Fig 6 A,B,). These changes in expression are not because these genes are weakly expressed in the embryo because when we examine the mapped reads, we fine a large number of mapped reads spanning the coding sequence of these de-repressed genes consistent significant levels of gene expression (Extended Data Fig 6 C'). These data suggest that de-repression of calcium/cAMP signaling and intestinal metabolism may be the underlying factor mediating the lasting changes we observe in reprogrammed progeny.

Given this effect on the expression of genes involved with intestinal digestion and lipid metabolism, we examined the role of *Hr96* in the reprogramming of progeny metabolism.

Hr96 encodes a nuclear receptor that the Drosophila ortholog of LXR and has been previously shown to function specifically in the intestine to regulate lipid digestion, trafficking, and storage, specifically in the intestine [26-28]. Consistent with this hypothesis, we found that eight known *Hr96* targets, including *mag(LipA), jon65Ai(protease), jon99Ci(protease), Jon65Aii(protease), CG9463(alpha-mannosidase), and CG15080* are de-repressed in the progeny of INR-DN expressing oocytes. We tested this hypothesis by feeding control flies and *Hr96/TM3* heterozygous flies a maternal amino acid-deficient diet, collecting the resulting control and *Hr96/Hr96* mutant progeny, and allowed them to mature on a standard diet (Extended Data Fig 6 E). This strategy allowed us to disrupt intestinal lipid metabolism, specifically in reprogrammed progeny, and determine if enhanced intestinal lipid metabolism promotes the life-long changes in adult metabolism we observe.

Interestingly, we found that disrupting *Hr96 in* progeny reduced the elevated levels of triglycerides and glucose we typically observe in the progeny from mothers fed an amino acid-deficient diet (Fig 4 K, M). Moreover, consistent with previous studies that show all *Hr96* mutant metabolic defects can be rescued by Hr96 expression in the intestine[26-28], we have found that Hr96 overexpression in enterocytes alone is sufficient to cause an increase in whole animal triglycerides similar to what is seen in reprogrammed progeny (Extended Data FIg 6 G). Taken together, these gene expression changes and functional studies with *Hr96* mutants support the model that the reprogramming of intestinal metabolism is a significant factor in the systemic metabolic changes seen in reprogrammed progeny.

Using ChIP-sequencing analysis, we found that most Polycomb complex regulated genes such as hox genes *abd-A* and *Antp* display normal levels of H3K27me3 (Fig 5A and Extended Data Fig 7C). However, many genes de-repressed in reprogrammed embryonic progeny, including *Jon74E, CG7542*, CG6295, and *magro*, display a loss (or reduction) of H3K27me3 specific peaks (red boxes) in the local genomic landscape (Fig 5 B&C) (Extended Data Fig 7 D). We also saw a corresponding increase in the activating mark H3K27-ac at these loci (Fig 5 B-D). We did not observe changes in H3K9 methylation in the genomic landscape of de-repressed genes (Fig 5 A-D). These data are consistent with the idea that a loss of H3K27me3 peaks or changes in nucleosome positioning activates specific silent regulatory sequences for metabolic transcription factors, such as *Hr96*, in the genomic landscape of key intestinal metabolism genes, causing their de-repression. In addition, when we examined the chromatin landscape of the calcium response gene *ARC1* and the Ca+ channel subunit *Ca-beta* we observed similar reductions in H3K27-me3 and corresponding increases in H3K27-ac in the genomic landscape consistent with their de-repression in the progeny of InR-DN expressing oocytes (Fig 5D)(Extended Data Fig 7E). Overall we propose that loss of H3K27-me3 allows for greater H3K27-ac and drives the de-repression of Intestinal genes and genes involved with CA+/cAMP signaling that underlies progeny metabolic reprogramming.

To examine if the de-repression of metabolic genes we observe in reprogrammed progeny stems from a global reduction of repressive heterochromatin *in vivo,* we examined how maternal amino acid diet impacted the process of position effect variegation (PEV). Reporters of position effect variegation, such as $ln(1)w^{m4}$, have been used for over 20

years to study factors that control global histone methylation[29]. Compared to controls that display low levels of eye pigment, an indicator of efficient silencing of the white gene by histone methylation, progeny reprogrammed by a maternal amino acid-deficient diet displayed higher levels of red-eye pigment (Fig 6A) (Extended Data Fig 7A). These data are consistent with the de-repression of the *white* gene due to lower levels of histone methylation. We examined global histone methylation by examining H3K27me3 and H3 in control and reprogrammed progeny using western blots. Consistent with our *in vivo* reporters, we observed a global (35%-65%) reduction in H3K27-me3 relative to the H3 levels in the embryonic progeny of InR-DN expressing progeny (Fig 6B and B'). Interestingly, we did not observe the same changes in chromatin state in InR-DN expressing oocytes (Fig 6 C & C') consistent with our model that reduced levels of NAD^+ drive chromatin changes in the early embryo to promote the reprogramming of progeny metabolism. As a means to determine the cause of this global reduction in H3K27-me3, we examined the production of the global methyl-donor S-adenosylmehtionine (SAM) by measuring the levels of intermediates in the methionine cycle (Extended data Fig 7B). We found a roughly 40% reduction in the levels of methionine, cysteine, Betaine, and SAM (Fig 6D) (Extended Data Fig 7B). This reduction in methionine cycle intermediates directly mirrors the reduction histone methylation we observe in reprogrammed progeny. Moreover, we found that supplementing reprogrammed progeny with exogenous methionine (3mg/ml) is sufficient to rescue the glucose and triglyceride phenotypes observed in the progeny from InR-DN expressing oocytes (Fig 6 E&F). To examine whether depletion of methionine cycle activity in progeny contributes to the metabolic reprogramming of progeny metabolism caused by NAD depletion, we fed progeny from NAPRT-RNAi expressing oocyte a methionine supplemented diet. We observed a similar rescue of the glucose phenotype we observed in the progeny of NAPRT-RNAi oocytes. We attempted to test the effect of the methionine cycle in progeny metabolic reprogramming genetically; however, inhibition of SAM-synthase causes severe lethal phenotypes. These data suggest that reduced levels of NAD+ in InR-DN oocytes causes compromised production of SAM by the methionine cycle in progeny. This depletion of SAM leads to loss of H3K27-me3 of intestinally expressed genes and reprogramming of intestinal metabolism (Fig 6 G). Moreover, this reduction in the methionine cycle is a significant factor causing the phenotypes observed in reprogrammed progeny. This model is consistent with the numerous studies showing that reduced levels of methionine cycle activity cause reduced histone methylation levels [30].

Quiescence has a conserved role in metabolic reprogramming.

To determine if the metabolic shifts during quiescence and progeny metabolic reprogramming are conserved in mammalian cells, we examined an established NIH 3T3 cell model of cellular quiescence[31]. Inducing cellular quiescence in 3T3 cells by reducing serum levels caused the same changes in mitochondrial respiration, glycolysis, and glycogen storage that we observed in *Drosophila* oocytes, suggesting that this model recapitulates the metabolic changes seen *in vivo as* germ cells enter quiescence (Fig 7A and B) (Extended Data Fig 8 A, A' and H). Restoring serum levels in these cultures reverses the suppression of mitochondrial metabolism in reactivated cells, similar to the metabolic changes that we observe as embryos emerge from quiescence (Fig 7B) (Extended data Fig 8B, B',F, and G). If we compare actively growing 3T3 cells with cells that were reactivated after a three-day

quiescent period and passaged twice, the reactivated cells display higher mitochondrial respiration and glycolytic activity (Fig 7 C, D, and I) (Extended Data Fig 8C and C'). We also observed changes in glycogen levels and the NAD^+/NADH ratio consistent with the reprogramming of progeny metabolism in *Drosophila* (Fig 7B) (Extended Data Fig 8D). These metabolic changes were not due to differences in cell number because total protein levels were not affected in these samples (Extended Data Fig 8E). These data are consistent with the model that quiescence has a conserved role in creating a metabolic environment that induces the reprogramming of progeny metabolism.

It has been shown that cellular quiescence in cancer cells provides a means to survive chemotherapy and give rise to recurrent tumors[32,33]. As a result, we wanted to determine if the quiescent nature of cancer cells that survive cisplatin-based chemotherapy treatment is also involved in the reprogramming of progeny metabolism. To test this idea, we treated MCF7 breast cancer cells with cisplatin for 48 hours to kill growing cancer cells and select for quiescent MCF7 cells. We then removed the cisplatin, washed the cells, and allowed them to recover and regrow to confluence for 12 days (Fig 7E). Analysis of the metabolic state of these cells revealed that recurrent MCF7 cells display increased mitochondrial respiration and glycolysis similar to that observed during progeny metabolic reprogramming in *Drosophila* and the 3T3 cell model for cellular quiescence (Fig 7 F, G, H). Interestingly, We also observed a reduction in methionine cycle intermediates (methionine, SAH, SAM) in recurrent MCF7 cells similar to our Drosophila model (Figure 8A). To determine the impact that metabolic reprogramming has on tumor growth, we injected these cells into Fox Chase SCID mice and examined the growth of xenograft MCF7 tumors. Interestingly, when we analyzed these tumors, they displayed a significant reduction in the levels of SAM similar to our observations in Drosophila (Figure 8B). Moreover, these tumors also displayed a modest increase in acyl-carnitine levels (Extended Data Fig 9B), consistent with the alterations we observed in mitochondria oxidative metabolism in recurrent MCF7 cells. Moreover, these data are consistent with reduced methionine cycle production of SAM in progeny being a critical factor in reprogramming progeny metabolic state in both *Drosophila* and mammalian models.

We examined chromatin status in recurrent MCF7 cells we found that the mouse orthologs of *ARC1* and *ca-beta, ARC* and *CACNB1*, as well as calmodulin 1 (Calm1), displayed a similar reduction in H3K27-me3 and a corresponding increase in the levels H3K27-ac to that which we observed in calcium signaling genes de-repressed in reprogrammed progeny in *Drosophila* (Fig 8 D-F). Given that we observed a de-repression of genes in the adult intestine in our *Drosophila* model, we hypothesized that we might observe a similar shift in chromatin landscape surrounding genes involved with mature mammary tissue in our recurrent MCF7 cells. Consistent with this idea, we observed lower H3K27-me3 and increased H3K27-ac in the genomic landscape of KRT18 and the promoter of *Esr1*(Extended Data Fig 8 C&D). We also observed a similar reduction in H3K27-me3 in the promoter regions of tumor suppressor genes such as *BRCA1*(Extended data Fig 9E) and *BRCA2*(Extended Data Fig 9F), suggesting they are depressed as well. If we look genome-wide, we observe a reduction in the number of H3K27-me3 peaks (~20-25%) similar to the reduction in H3K27-me3 observed in Drosophila reprogrammed progeny (Extended data Fig 9A). Overall, these data suggest that progeny metabolic reprogramming may push the

recurrent cells to a more differentiated state and impair the aggressive growth of recurrent tumors. Consistent with this model, we observed a significantly slower growth of recurrent MCF7 tumors in our mouse xenograft model (Figure 8C). Overall, these studies support the idea that cellular quiescence has a broad role in establishing a metabolic state the supports the reprogramming of progeny metabolism. In reproductive systems, this mechanism drives a transgenerational shift in progeny metabolism. In contrast, in somatic cells, it may function at the cellular level to promote the disfunction of adult stem cell and their descendants and reprogram mitochondrial metabolism in models of cancer recurrence.

Discussion

Many studies have shown that maternal metabolic stress can significantly impact progeny metabolic state and disease susceptibility. [5-7]. While many studies have examined the lasting changes in progeny physiology, few studies have examined the heritable factors in germ cells that drive progeny reprogramming[34,35]. Our data show that non-DNA factors such as metabolites can function as heritable factors that drive progeny metabolism. Our data also show that changes in NAD metabolism contribute significantly to progeny reprogramming by causing reduced methionine cycle activity and reduced production of the methyl-donor SAM in progeny. These data are consistent with the well-established requirement of NAD^+ by the methionine cycle enzyme S-Adenosyl-homocysteine hydrolase.

Upon examining H3K27me3 mediated repression reprogrammed progeny, we found a significant reduction in H3K27me3 levels, specifically in reprogrammed embryonic progeny. Along with a decrease in total methylation, using ChIP-sequencing analysis of repressive chromatin marks, we observed a loss of specific H3K27-me3 peaks and a shift in H3K27-me3 nucleosome positioning in the genomic landscape of many intestinal metabolism genes that are de-repressed in the reprogrammed progeny. These data indicate that the critical period for progeny reprogramming occurs during early embryogenesis when the chromatin state during embryonic development is highly flexible in many systems.

Previous studies have shown that maternal metabolic stress can significantly impact stress tolerance in progeny [36-39]. Our data show that this reprogrammed metabolic state supports growth in a poor nutrient environment. When we place reprogrammed progeny on a standard diet, they manifest defects in triglyceride metabolism and glucose homeostasis as adults. These metabolic defects likely stem from an incompatibility between the metabolic state of reprogrammed progeny and the nutrient-rich environment, which drives the shortened life span we observed in reprogrammed progeny. Consistent with this, in the case of the Dutch famine, the mothers were subject to famine but the resulting children grew with a regular ad libitum diet. It is possible that removing metabolic stress in the progeny generation causes incompatibility between metabolic programming of progeny and the nutrient environment that contributes to disease and a shortened lifespan.

Interestingly, the quiescent nature of germ cells provides a unique state where metabolic stress can induce reprogramming of cellular metabolism. Studies from several systems have shown that quiescent cells are both transcriptionally and translationally silent [40-42]. As a result, many of the mechanisms that respond to metabolic stress are compromised during

this dormant period. Our work in *Drosophila* shows that nutritional stress in germ cells causes a precocious activation of the metabolic program that supports quiescence (MRQ). The blunted ability of quiescent cells to respond to metabolic changes, in conjunction with sweeping changes in mitochondrial metabolism that occur during MRQ, that help create significant changes in NAD+ redox metabolism that drive progeny reprogramming. In active cells, severe NAD^+ depletion would either kill the cell or trigger increased NAD^+ regeneration and biosynthesis to correct the problem quickly. Our model suggests cellular quiescence provides a state where cells can tolerate high levels of reductive stress and establishes an environment conducive to the reprogramming of progeny metabolic states.

Using a NIH3T3 cell model for quiescence[31] , we found that inducing a transient period of quiescence reprograms progeny metabolism Identically to what we observe in *Drosophila* embryos suggesting quiescence has a conserved role in metabolic reprogramming. Interestingly, during cancer recurrence, subsets of cancer stem cells enter quiescence and survive chemotherapy [33]. In a fraction of chemotherapy treatments, these recurrent cells drive cancer recurrence. [32,43]. We have found that recurrent MCF7 cells display a reprogrammed metabolic highlighted by a dramatic increase in mitochondrial oxidative metabolism. This increase in respiration coincides with reduced H3K27-me3 in the genomic landscape of calcium signaling genes and genes expressed in mature breast tissue suggesting these reprogrammed cells may be closer to a differentiated state. Consistent with these observations, recurrent MCF7 cell xenograft tumors display a significantly reduced growth rate, suggesting that progeny metabolic reprogramming may be an obstacle to aggressive recurrent growth that an aggressive recurrent tumor would have to overcome by accumulating other oncogenic mutations. These observations are consistent with previous studies that suggest metabolic regulators such as PGC-1alpha impact cancer recurrence and chemotherapy sensitivity[44,45].

By directly examining the biochemical changes in quiescent oocytes, our work provides several key insights into how cellular quiescence is directly linked to the reprogramming of progeny metabolism. First, maternal metabolic stress causes the premature onset of MRQ and disrupts the unique redox state of quiescent oocytes. Second, we show that changes in a specific metabolite in quiescent oocytes, NAD^+, serves as a heritable factor that drives progeny reprogramming. These findings provide an intriguing new model for how non-DNA factors can induce cellular reprogramming events. In contrast to the conventional view of cellular quiescence as simply a dormant and protective state, our work highlights that cellular quiescence creates a physiological state that facilitates the remodeling of the chromatin landscape.

Methods

Contact for Reagent and Resource Sharing

Further information and requests for resources and reagents should be directed to and will be fulfilled by the Lead Contact, Matthew Sieber (matthew.sieber@utsouthwestern.edu)

Data Sharing

RNA seq and ChIP data have been deposited under accession numbers: GSE145353, GSE175387 GSE175754, GSE175755, and GSE175756. All other data will be provided upon request.

Experimental Model and subject details

Drosophila melanogaster stocks.—UAS-NAPRT-RNAi(HMJ23364), UAS-NAPRT-RNAi(HMC05271), UAS-InR-DN(8252), UAS-InR-DN(8253), UAS-roGFP(67665, and UAS-TOR-DN(7013) fly lines were obtained from the Bloomington Drosophila stock center. The MTD-GAL4 line was obtained from Lynn Cooley(Yale). The Hr96 mutant lines and uas-Hr96 transgenic lines were obtained from Carl Thummel(Univ. Utah).

Normal and modified dietary treatments—To ensure reproducibility, we used an amino acid-deficient grape agar media previously published to suppress insulin release from the IPCs. This media is commercially available from Genesee Scientific (cat# 47-102). The control diet is a standard drosophila culture media that contains 336g agar, 630g yeast, 2520g cornmeal, 3360ml molasses, and 33.4L of H_2O. Antifungals (Tegosept and propionic acid) were added after food has cooled to 60C.

*** Rich media described in figure 1 is made by adding ~1gram of yeast paste to the bottle control food described above.

**** low-nutrient media mentioned in figure 1 was made by taking 100 ml of control media and diluting it 3/1 with 1% agar and water. This yields a food with 1/3 the nutrient value of control food.

Cell lines

NIH 3T3 cells (ATCC CRL-1658) and MCF7 cells (ATCC HTB-22) were cultured in DMEM (+10% FBS) at a temperature of 37C with 5% CO_2.

TMRE staining

Dissected ovarioles were incubated in 1xPBS with10 nM TMRE for 5 mins. Oocytes were then washed 4 times in 1xPBS and mounted on slides in 1xPBS. The oocytes were imaged immediately using fluorescence and DIC via confocal microscopy.

TAG measurements

TAG levels were measure using samples of 10 adult flies homogenized in 200ul 1XPBST. TAG levels were measured precisely as described in Sieber and Spradling 2013 using Sigma triglyceride reagent and sigma free glycerol measurements. Total protein levels were measured, and the samples were normalized. The data is displayed as a percentage relative to the control samples.

Catalog numbers

Sigma Triglyceride Reagent cat# **T2449-10ML**

Free Glycerol reagent cat # **F6428-40ML**

Glycerol standard cat# **G7793-5ML**

Glucose/glycogen assays

Glucose and glycogen levels were measured using samples of 10 adult flies homogenized in 200ul 1XPBST. Glucose/glycogen levels were measured exactly as described in Sieber et al (Cell 2016) using a Sigma Glucose oxidase Kit. Total protein levels were measured, and the samples were normalized total protein and displayed as a percentage of control.

LC/MS metabolomics

Samples of 300 oocytes and wash 2x with fresh 1xPBS. Samples were then snap-frozen in liquid nitrogen and store at −80°C until analysis. Samples were weighed and then homogenized in 1 ml of methanol: H_2O (80:20). The sample was then vortexed for 2 mins and then centrifuged ~20,000xg for 15mins. The pellet was kept for protein normalization and the supernatant dried down by low temp speedvac. The resulting dried samples were then frozen at −80C until analyzed.

LC/MS analysis

Samples are analyzed by targeted LC/MS metabolomics with the assistance of the UT Southwestern metabolomics facility (https://cri.utsw.edu/facilities/metabolomics-facility/). Using Sciex SIMCA software, we will analyze these data sets and perform Partial Least Square analysis to examine sample clustering. From the PLS analysis, we will identify metabolites that exhibit a high VIP score (>1.0) as candidate compounds that contribute to the reprogramming of progeny metabolism. The data is compiled from 8 independent samples/conditions to accurately represent the biological variation of the experiment and provide sufficient statistical power.

GC/MS metabolomics analysis

All GC/MS metabolomics analysis was conducted exactly as described in (Sieber et al. 2016). Samples were then collected at 300 oocytes/sample and flash-frozen in liquid nitrogen, and stored at −80C until processed. Vials containing oocytes were removed from −80°C freezer, and the contents immediately transferred into a bead mill tube containing 1.4 mm ceramic beads (MoBio Laboratories, Carlsbad, CA). This tube contained 400 µL of 80% MeOH that had been chilled to −20 °C. Whole flies were homogenized for 30 seconds at 6.5 m/sec with an Omni Bead Ruptor 24 bead mill (Omni-Inc, Kennesaw, GA). Cell debris was removed by centrifugation at 14000 x g for 5 minutes at 4 °C. The supernatant was transferred to microcentrifuge tubes, and the solvent was removed *en vacuo*.

GC-MS analysis was performed with a Waters GCT Premier massspectrometer fitted with an Agilent 6890 gas chromatograph and a Gerstel MPS2 autosampler. Dried samples were resuspended in 40 µl of a 40 mg/mL O-methoxylamine hydrochloride (MOX) in pyridine and incubated for one hour at 30°C. 25 µl of this solution was added to each autosampler vial. Ten microliters of N-methyl-N- trimethylsilyltrifluoracetamide (MSTFA) was added automatically via the autosampler and incubated for 60 minutes at 37°C with shaking. After

incubation 3 μl of a fatty acid methyl ester standard solution was added via the autosampler. 1 μl of the prepared sample was injected into the gas chromatograph inlet in the split mode at a 10:1 split ratio with the inlet temperature held at 250°C. The gas chromatograph had an initial temperature of 95°C for one minute followed by a 40°C/min ramp to 110°C and a hold time of 2 minutes. This was followed by a second 5°C/min ramp to 250°C, a third ramp to 350°C, then a final hold time of 3 minutes. A 30 m Phenomex ZB5-5 MSi column with a 5 m long guard column was employed for chromatographic separation

Data was collected using MassLynx 4.1 software (Waters). A two-step process was employed for data analysis, a targeted followed by non-targeted analysis. For the targeted approach known metabolites were identified and their peak area was recorded using QuanLynx. This data was transferred to an Excel spread sheet (Microsoft, Redmond WA). Metabolite identity was established using a combination of an in-house metabolite profile library developed using pure purchased standards and the commercially available NIST library. When reporting each metabolite those with absolute identity are not qualified, those that are identified using a NIST library are noted using a percentage of certainty produced by the NIST software.Not all metabolites are observed using GC-MS. This is due to several reasons, one being that they present at very low concentrations. A second is they are not amenable for the GC-MS procedure due to either being too large, too volatilize, are a quaternary amine such as carnitine, or do not properly ionize. Metabolites that do not ionize well include oxaloacetate and arginine. Cysteine was observed depending upon cellular conditions, it often forms disulfide bonds with proteins and is at low intracellular concentration. Statistical analysis was performed using MetaboAnalyst Ver. 2.. data was converted to .csv file and uploaded into the MetaboAnalyst server. data was mean filtered to remove variables of very small values, normalized by autoscaling, and fold change, t-test and volcano plot were generated.

The data is compiled from 10 independent samples/condition to accurately represent the biological variation of the experiment and provide sufficient statistical power.

RNA sequencing

7-day old flies were dissected and oocytes collected in Grace’s insect medium. 200 oocyte/embryo were collected per sample. Each experimental condition was collected in triplicate. Samples were homogenized and 600uL fresh tripure added. Samples then rested at room temperature for 10 minutes. 180uL chloroform was added and samples shaken by hand for 45 seconds followed by room temperature incubation for 10 minutes. Samples were then centrifuged for 15 minutes at 12,000 rpm at 4°C, and the aqueous layer moved to a fresh tube. RNA was then precipitated with 400 uL isopropanol. RNA was spun down at 12,000 rpm for 15 minutes at 4°C and the liquid removed. The pellet was washed twice with 75% ethanol and then air dried for 5 minutes. RNA was resuspended in 50uL nuclease free water and stored at −80°C.

Sequenced reads were analyzed using the Tuxedo Suite (TopHat, Cufflinks and cuffdiff). We focused our analysis on genes whose expression was greater than 2 FPKM and a q-value <0.05. Genes reported as significantly changing had at least 1.5 fold changes in expression.

ChIP-sequencing analysis

20 mg of cells (~300 eggs) were homogenized and fixed in 1% formaldehyde with frequent shaking for 15 min at room temperature. After quenching with 250 mM glycine and washing 3 times with ice-cold PBS, the samples were sonicated with a 1/8-inch probe (15 seconds on/25 seconds off, 30 cycles, 25% of maxi power) by sonicator (Branson 550) to obtain genomic DNA fragments with an average size of 150-250bp. Chromatin IP (ChIP) was performed following the protocol provided by Millipore ChIP Assay kit (Millipore, 17-295). Briefly, the 1.5ml sonicated lysates were incubated with 1.5 μg H3K27me3 antibody (Millipore, 07- 449), , H3K27-ac (Cell signaling #8143-s), or 1.5 μg H3K9me3 antibody (Abcam, ab8898) overnight at 4C. The next day, 60 μl protein A magnetic Dynabeads beads (Life Technologies, 10004D) was added and incubated for 3 hours to pulldown chromatin complex. After washing and de-crosslinking at 55C for 4h, the precipitated DNA was purified using a ChIP DNA clean & concentrator (Zymoresearch, D5201). The ChIP libraries were prepared following ThruPLEX® DNA-Seq Kit (Takara, R400674) with 10 PCR amplification cycles. The libraries were then sequenced using an Illumina HiSeq500 with single-end and 75 bp read length. Quality control for these samples was assessed using FASTQC. The resulting reads were mapped using Bowtie2. HOMER was used to call and annotate the peaks in our ChIP-seq data. These data were analyzed with help from the UTSW bioinformatics lab.

Q-PCR Primers

The following is a list of Q-PCR primers used in this study:

magro fp 5'-GTGTACCTGGTGATGCTTTCC-3' , rp 5'-CGACGATCTTGCTGAGATCG-3',

CG6295 fp 5'-GTCCGTGACCGAGAACAACT-3', rp 5'-TTAGTTGCCCATTCCGTAGG-3'

ARC1 fp 5'-ATCATCGAGCACAACAACCA −3', rp 5'- CTACTCCTCGTGCTGCTCCT −3'

ca-beta fp 5'-CAACAAGGAGAAGCGAAAGC-3', rp 5'-GGTGCTTGAGGAAGTCGAAG-3'

NADK fp 5'-AGGTGACCAATGTCCTGGAG-3' rp 5'-TTGAGCTGCCTTTGGAAACT-3'

NAAM fp 5'-GAGCGCCTTGAGCAGATATT-3', rp 5'-ATGGGCTCCAGTATCTCGTG-3'

NADsyn fp 5'-AGCCCTACAAACGGAGGAGT-3', rp 5'-ACATCTCGATGTGCTTGCTG-3'

fluorescence quantification

Quantified Delta fluorescence reported in Extended Data 3 was measured using the integrated density measurement in ImageJ. Corrected total cell fluorescence was calculated by subtracting mean fluorescent background from the same image.

3T3 cell model for Quiescence

3T3 cells were cultured in DMEM(+10%FBS) until 90% confluent. Mediate was removed and cells were rinsed 2X in 1xPBS. Fresh starvation media was added (DMEM+.1% FBS) and cell were incubated for 3 days. Starvation media was then removed and fresh DMEM(+10%FBS) was added. After 2 days of reactivation cell were then plated on a seahorse assay plate and OCR and ECAR were measured.

MCF7 cisplatin resistance protocol

MCF7 cells were cultured in DMEM (+10%FBS) until 85-90% confluent. Cisplatin (sigma# PHR1624) was then added to the media for a final concentration of 50ug/ml. The resulting plates were incubated for 48hrs. More 95% of cell are killed by apoptosis in this procedure. After 2 days the plates were rinsed with 1xPBS and fresh DMEM (+10%FBS). Allow cells to recover and grow for approximately 14 days transferring media as needed. These recover cells were then plated on seahorse assay plates and assayed for OCR and ECAR.

MCF7 Xenograft injections

Our mouse xenograft experiments were done following our UTSW IACUC approved mouse protocol (Sieber protocol# 2020-102956). A 14-hour light/10-hour dark cycle facility maintained at 22°C and 50%humidity. Mice were fed a standard chow diet. Female Fox Chase SCID mice (Charles River) (3 months of age) were anesthetized and injected with 1 Million MCF7 cells into mammary tissue below the 4^{th} nipple on the left side. Estradiol was administered at (4mg/kg) bodyweight weekly to support tumor growth. Tumor size was measured twice weekly to track tumor growth. In line with our IACUC protocol we did not allow tumors to exceed 2cm in diameter. Once tumors reach roughly $40mm^2$ tumor volume, they were collected, weighed, and used for subsequent metabolite measurements. These experiments were done with assistance from the UTSW animals resource center and reflect 2 independent sets of injections from 2 independent isolations of recurrent MCF7 cells. A total of 16 mice/condition were assayed.

Seahorse analysis

The day before assay each well is plated with 15,000 cells per well. One the day of the assay cell culture media is removed and replaced with seahorse assay media supplemented with glutamine. Cells are allowed to acclimate to assay media for 2 hrs in the incubator. Once acclimated the cells are assayed for basal OCR, ATP-dependent OCR, and maximal OCR using a standard mito-stress kit protocol. For the assay we used 2uM oligomycin and 1uM FCCP for the injections. Once the assay is complete cells are collected and total protein levels ae measured by Bradford protein assay to ensure the observed changes in respiration do not manifest from changes in cell number. All experiment were conducted on a Seahorse XFp machine.

Abbreviations

MRQ mitochondrial respiratory quiescence

Quantification and statistical analysis

All metabolite measurements are conducted on at least 8 biological replicate samples per experiment and each experiment is replicated at least 3 times unless stated otherwise. All error bars represent standard deviation of the sample group. Significance values are calculated by students t-test for pairwise comparisons and One-way ANOVA with a post-hoc Tukey correction for experiments where more than 2 samples groups are compared.

Extended Data

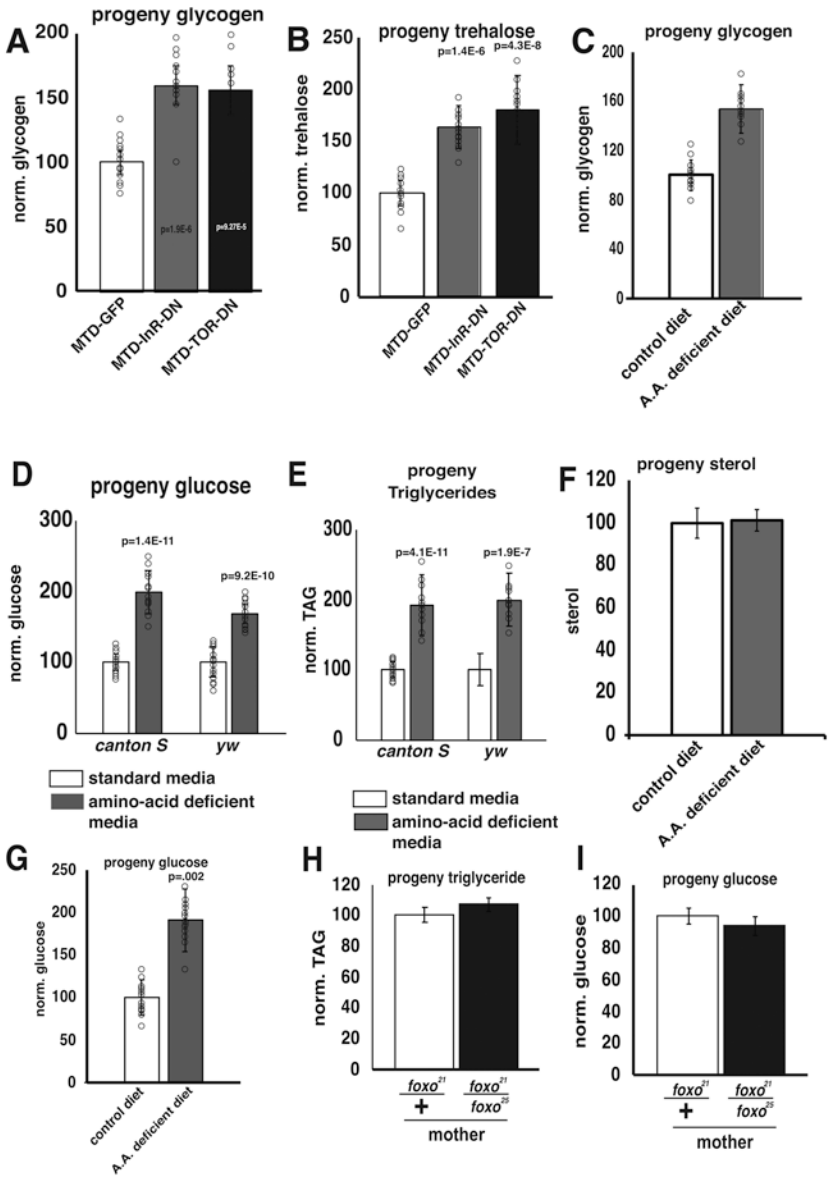

Extended Data Fig. 1. Metabolic profiling of reprogrammed progeny

A) Glycogen levels in progeny from MTD-GFP, MTD-InR-DN, and MTD-TOR-DN mothers fed control or an amino acid-deficient diet(n=10 biological replicates, p=1.9E-6, p=9.27E-5 calculated by one way anova). B) Normalized trehalose levels in progeny from

control, InR-DN, and TOR-DN expressing oocytes (n=10 biological replicates, p=1.4E-6, p=4.3E-8 calculated by one way anova). C) Adult glycogen levels from the progeny of parents fed either an amino acid-deficient media or a control media (n=10 biological replicates). D) A graph showing diet can induce reprogramming of glucose metabolism in *yw* and *Canton S* genetic backgrounds (n=10 biological replicates, p=1.4E-11, p=9.2E-10 calculated by students t-test). E) A graph showing diet can induce reprogramming of triglyceride metabolism in *yw* and *Canton s* genetic backgrounds(n=10 biological replicates, p=4.1E-11, p=1.9E-7 calculated by students t-test). F) sterol levels in progeny from mothers fed control or an amino acid-deficient diet(n=10 biological replicates). (G) Glucose levels from the progeny of mothers fed either a control diet or an amino acid-deficient diet(n=10 biological replicates, p=0.002 calculated by students t-test). (H, I) Graphs showing that *foxo* does not induce the reprogramming of progeny glucose and triglyceride metabolism(n=10 biological replicates). Error bars represent 1X standard deviation.

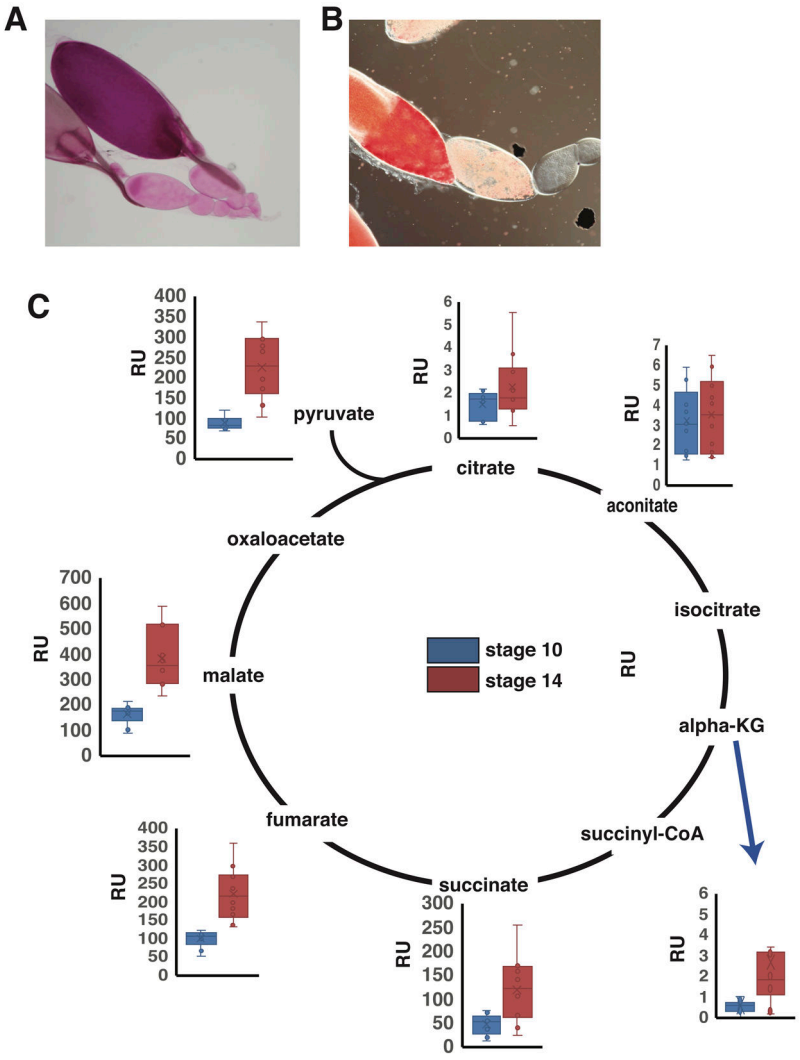

Extended Data Fig. 2. Changes in TCA cycle profile during quiescence

A) Glycogen (PA/S staining) staining for wild-type ovarioles. B) Oil Red O staining of wild-type ovarioles. C) A summary of GC/MS data characterizing the TCA cycle changes that occur as oocytes mature and enter quiescence. (n=10 biological replicates) (Box and whisker plots= The box represents the upper/lower quartile of the data presented the line within the box is the mean of the data presented. The whisker represent the maximum and minimum of the data.). Error bars represent 1X standard deviation

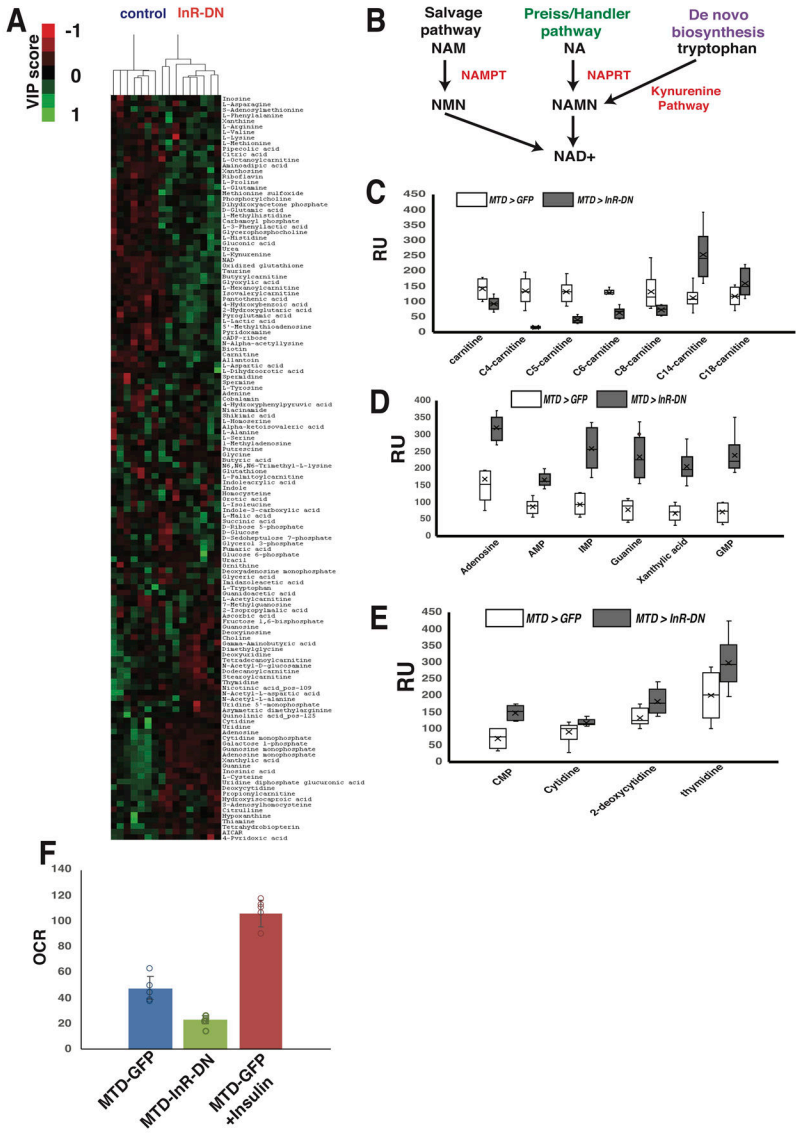

Extended Data Fig. 3. Metabolism changes in InR-DN expressing oocytes

A heat map of LC/MS metabolomic data displaying the VIP score of metabolites assayed in our metabolic data. B) A model displaying the mechanisms that produce NAD+. C) LC/MS data showing changes in fatty-acyl carnitines in control (*MTD>GFP*) and InR-DN expressing oocytes. D) Purine levels in control and InR-DN expressing oocytes. E) Pyrimidine levels in control and InR-DN expressing oocytes. (Box and whisker plots= The box represents the upper/lower quartile of the data presented the line within the box is the

mean of the data presented. The whisker represent the maximum and minimum of the data.) F) OCR measurements of follicles from MTD-GFP, MTD-InR-DN, and MTD-GFP follicles cultured with 10 ug/ml Insulin).

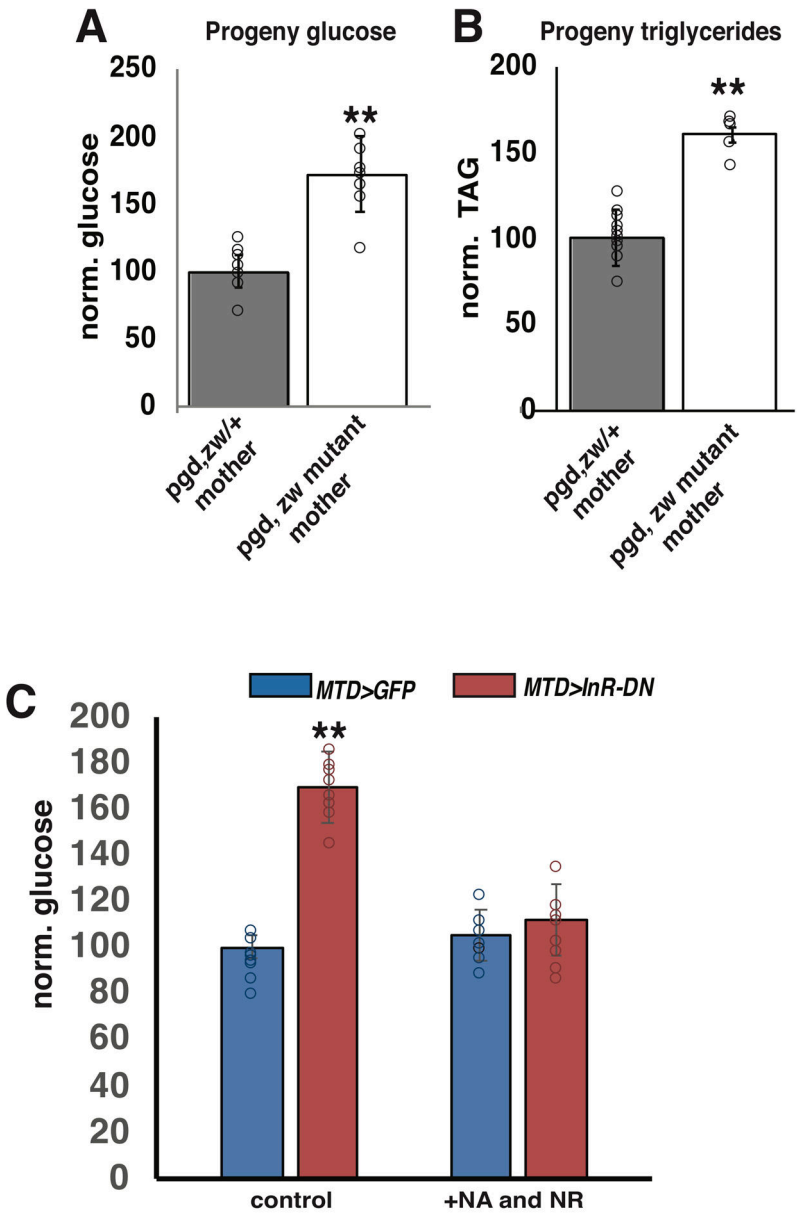

Extended Data Fig. 4. Metabolite measurements from mutants lacking a functional pentose phosphate pathway

Glucose levels (A) and triglyceride levels (B) from adult progeny produced from crossing *Pgd,zw/+* or *Pgd,zw/Pgd,zw* virgins to *Oregon R* males(n=10 biological replicates). C) Normalized glucose levels from control and InR-DN expressing progeny that were supplemented with a combination of NA (2mg/ml) and NR (2mg/ml) (n=12 biological replicates) Error bars represent 1X standard deviation.

A

GENE_NAME	logFC	logCPM	LR	PValue	FDR	maternally loaded
nej	-2.264318	9.050697	42.50457	7.05E-11	3.82E-09	Y
jim	-2.010455	4.759146	13.61477	0.000224	0.002681	N
spen	-1.812869	8.844686	40.81198	1.68E-10	8.50E-09	Y
Hers	-1.679205	5.968389	25.37159	4.73E-07	1.23E-05	Y
ranshi	-1.458669	3.17974	28.52756	9.24E-08	2.77E-06	Y
dikar	-1.371103	7.126167	44.38829	2.69E-11	1.53E-09	Y
tou	-1.367796	8.28302	28.68304	8.52E-08	2.58E-06	Y
fs(1)h	-1.352887	8.960666	26.21279	3.06E-07	8.32E-06	Y
Gug	-1.269078	8.338429	32.44025	1.23E-08	4.43E-07	Y
pygo	-1.266546	7.234263	45.95941	1.21E-11	7.09E-10	Y
pgc	-1.246593	7.527957	31.16142	2.37E-08	8.11E-07	Y
skd	-1.241762	8.424606	31.85044	1.67E-08	5.91E-07	Y
BRWD3	-1.212112	7.969835	33.03055	9.07E-09	3.40E-07	Y
Mi-2	-1.199995	9.444266	19.11504	1.23E-05	0.000217	Y
CG8677	-1.18063	8.027473	30.37116	3.57E-08	1.19E-06	Y
lilli	-1.178032	6.983042	39.11788	3.99E-10	1.88E-08	Y
polybromo	-1.170321	8.090431	22.43872	2.17E-06	4.76E-05	Y
Trl4-1	-1.169873	7.300613	31.65297	1.84E-08	6.46E-07	Y
Atu	-1.159918	6.981899	10.70567	0.001068	0.009535	Y
CG32767	-1.155885	7.743642	35.41228	2.67E-09	1.11E-07	Y
H	-1.151638	7.116219	39.72328	2.93E-10	1.40E-08	Y
gpp	-1.130552	7.851006	32.53127	1.17E-08	4.27E-07	Y
CG31224	-1.123516	7.54261	33.35474	7.68E-09	2.94E-07	Y
Bap170	-1.116479	7.427912	32.79257	1.03E-08	3.76E-07	Y
zfh1	-1.117234	6.418239	25.16449	5.26E-07	1.34E-05	N
MESR4	-1.110072	7.329404	33.01212	9.16E-09	3.43E-07	Y
Camta	-1.109491	5.235707	18.75518	1.49E-05	0.000259	Y
N	-1.109592	8.403342	24.95674	5.86E-07	1.48E-05	Y
CG5098	-1.098227	6.130407	31.77871	1.73E-08	6.10E-07	Y
trr	-1.092413	6.726685	35.15541	3.04E-09	1.25E-07	Y
CG12299	-1.054164	6.116364	28.35304	1.01E-07	2.99E-06	Y
brm	-1.048545	8.239644	24.76578	6.47E-07	1.61E-05	Y
E(Pc)	-1.045838	8.41552	23.86092	1.04E-06	2.47E-05	Y
Blimp-1	-1.044467	2.734088	16.29782	5.41E-05	0.000797	N
CG1815	-1.041184	6.338608	29.8502	4.67E-08	1.50E-06	Y

B

Term	PValue
Coiled coil	7.40E-21
Alternative splicing	3.97E-15
Phosphoprotein	7.39E-13
splice variant	3.24E-11
Developmental protein	9.39E-09
compositionally biased region:Gln-rich	9.41E-08
Cytoplasm	1.14E-07
imaginal disc-derived morphogenesis	3.27E-07
compositionally biased region:Ala-rich	5.45E-07
compositionally biased region:Ser-rich	1.30E-06
Metal-binding	1.36E-06
imaginal disc leg morphogenesis	3.50E-06
Zinc finger, PHD-type, conserved site	7.25E-06
Bromodomain	8.97E-06
EGF-like domain	1.78E-05
P granule	1.80E-05
Pleckstrin homology-like domain	2.22E-05
Zinc finger, PHD-finger	2.83E-05
Zinc finger, FYVE/PHD-type	3.17E-05
long-term memory	3.26E-05
Calcium	4.59E-05
actin filament organization	4.91E-05

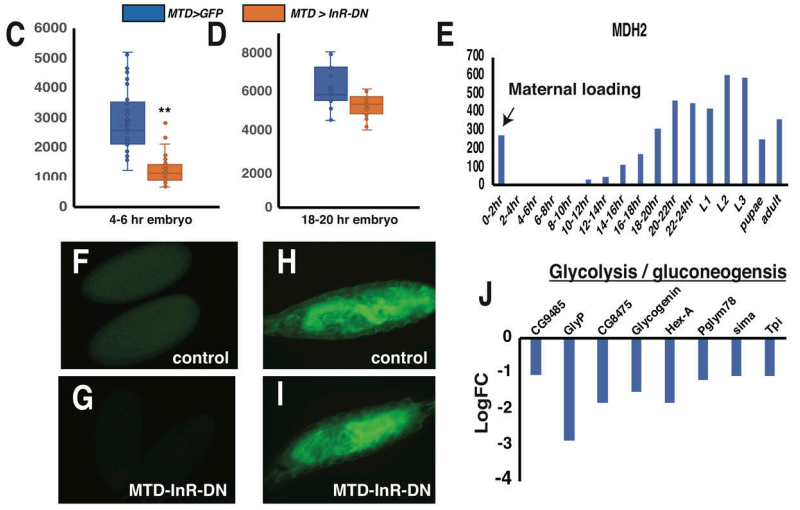

Extended Data Fig. 5. Gene expression changes in InR-DN expressing oocytes.

A) A table showing the known transcriptional regulators that are down-regulated in quiescent oocytes. B) Gene ontology analysis of the genes downregulated in InR-DN oocytes. (C, G, F) Redox reporter expression in early embryos (4-6 hrs) derived from control and InR-DN expressing oocytes. D,H,I) Redox reporter expression in late embryos (16-20 hrs) derived from control and InR-DN expressing oocytes(n=30 biological replicates) (Box and whisker plots= The box represents the upper/lower quartile of the data presented the line within the box is the mean of the data presented. The whisker represent the maximum and minimum of the data.). E) Developmental expression of MDH2 showing that this gene is maternally loaded. J) A graph showing that glycolysis and gluconeogenesis genes are down-regulated in quiescent oocytes. Error bars represent 1X standard deviation

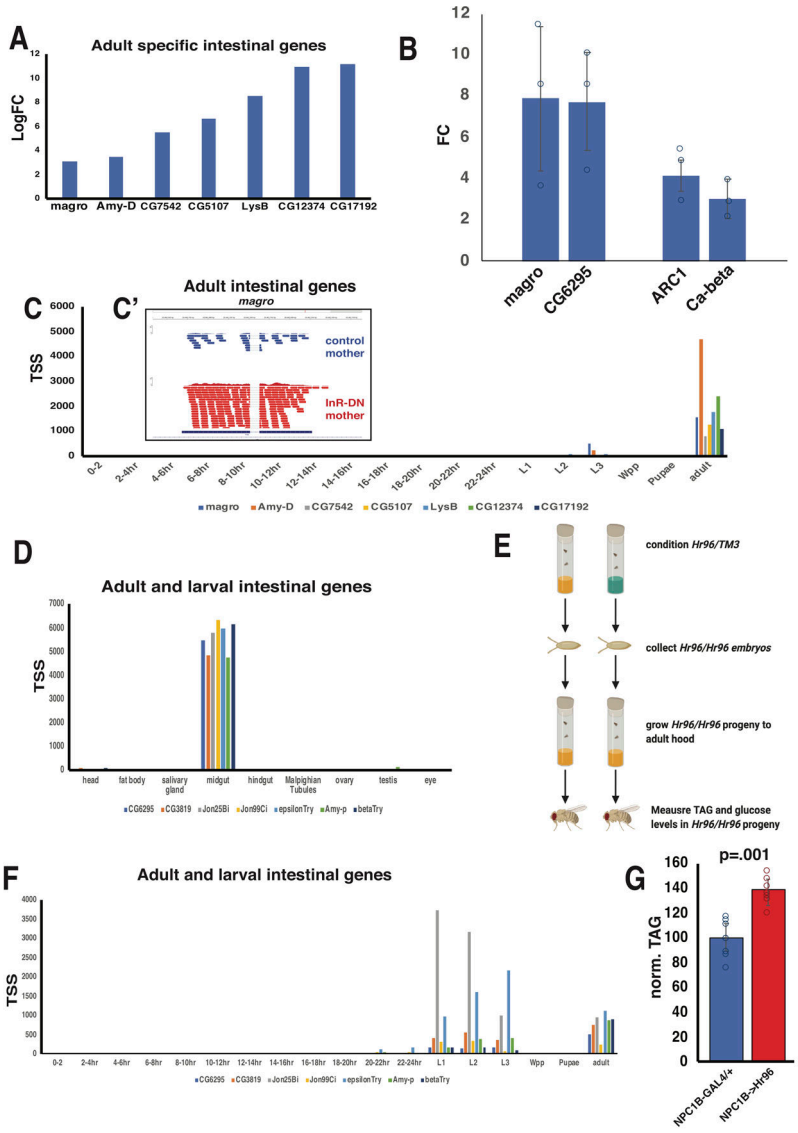

Extended Data Fig. 6. De-repression of intestinal metabolism genes in reprogrammed progeny

A) A graph highlighting 7 adult-specific intestinal genes that are de-repressed in Progeny of InR-DN expressing oocytes. B) Q-PCR validation of 2 intestinal gene and 2 calcium signaling genes de-repressed in InR-DN progeny (n=3 biological replicates). C) The developmental expression profile of 7 adult specific intestinal genes de-repressed in InR-DN progeny. C') RNA-seq mapped reads showing the expression levels of the intestinal gene *magro.* A graph showing examples of adult/larval-specific intestinal genes that are up-regulated in the embryonic progeny of InR-DN expressing oocytes. D) Tissue expression profile of seven adult and larval expressed intestinal genes that are up-regulated in the embryonic progeny of InR-DN expressing oocytes. E) Diagram of how Hr96 function was examined in reprogrammed progeny. F) The developmental expression profile of 7 adult and larval intestinal genes de-repressed in InR-DN progeny. G) Normalized triglyceride levels from flies overexpressing *Hr96* in the enterocytes (n=10 biological replicates, p=0.001, calculated by students t-test). Error bars represent 1X standard deviation

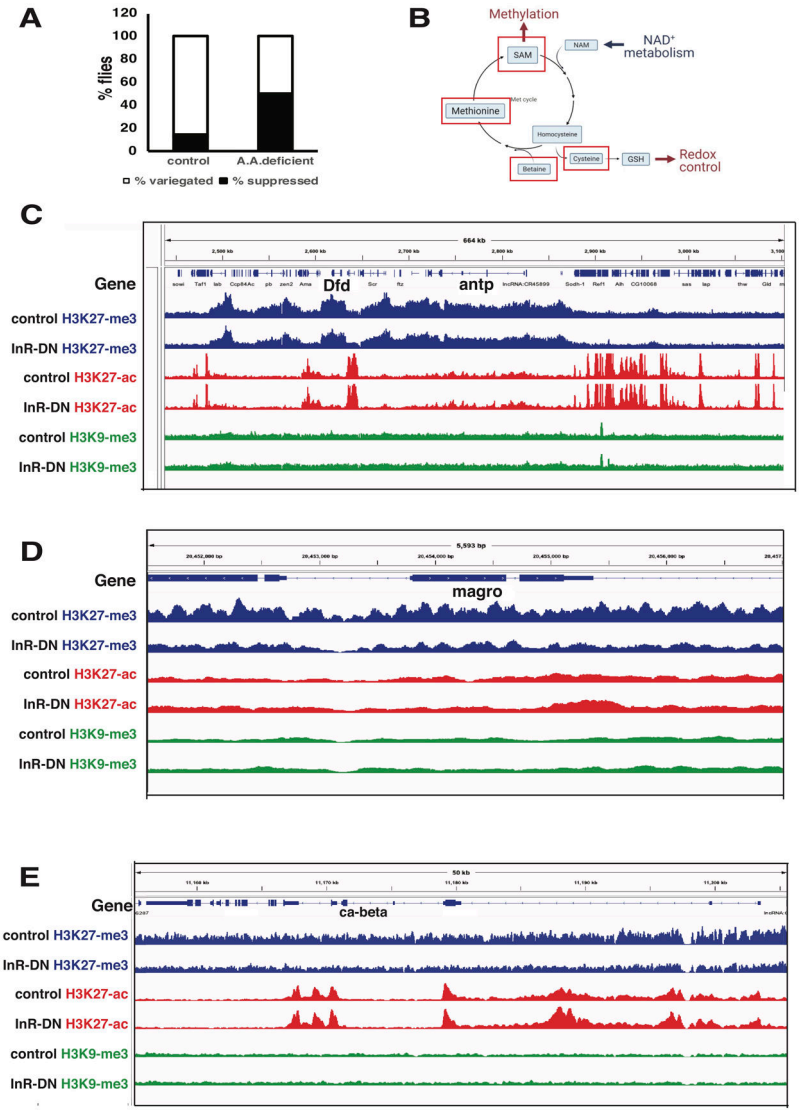

Extended Data Fig. 7. Chromatin changes in reprogrammed progeny

A) Quantification of relative levels of variegated and normal eyes (suppressed) in W^{m4} animals fed a control diet or an amino acid-deficient diet(n=275). B) A diagram of the methionine cycle. The intermediates that are reduced in reprogrammed progeny are highlighted with a red box. C) H3K27-me3, H3K27-ac, and H3K9-me3 ChIP seq profile of the genomic region that contains *antp*. D) H3K27-me3, H3K27-ac, and H3K9-me3 ChIP seq profile of the genomic region that contains *magro*.(red boxes represent genomic regions with altered histone methylation). E) H3K27-me3, H3K27-ac, and H3K9-me3 ChIP seq profile of the genomic region that contains *ca-beta.*

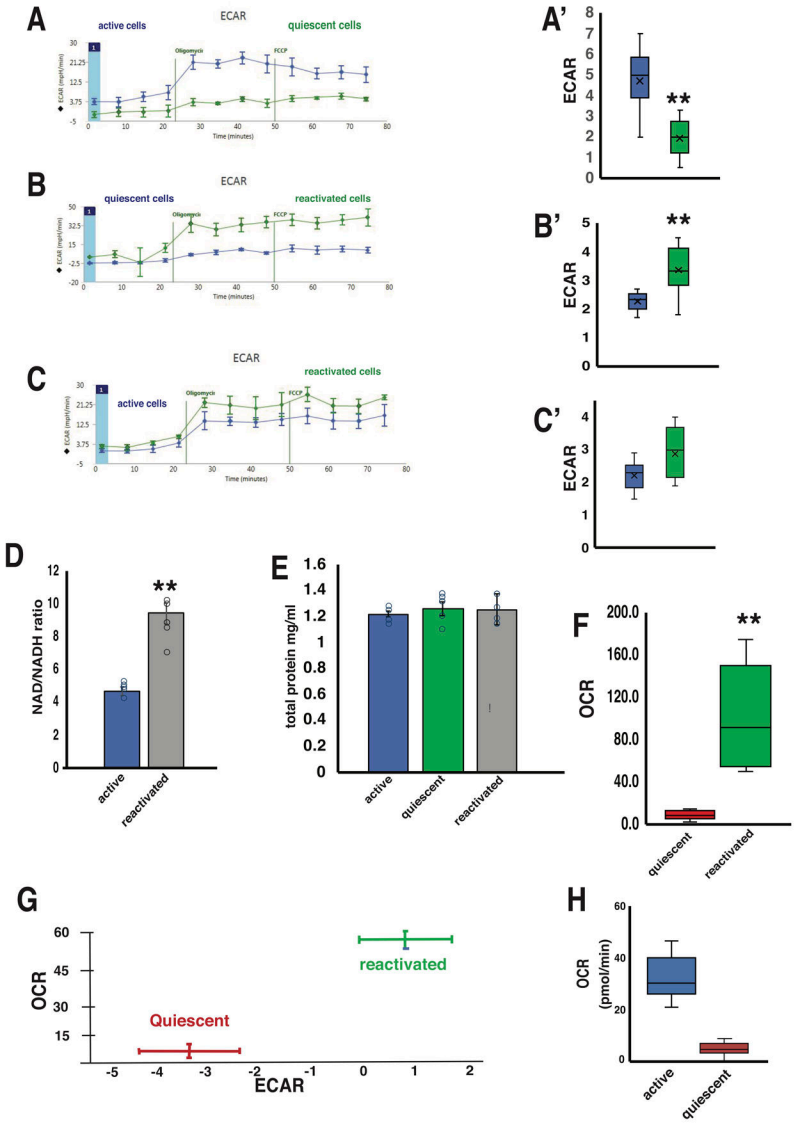

Extended Data Fig. 8. Mitochondrial analysis metabolic reprogramming in mammalian models.

A) An ECAR trace read comparing active and quiescent NIH 3T3 cells(n=9 biological replicates). A') ECAR data comparing active and quiescent cells compiled from multiple experiments(n=9 biological replicates). B) ECAR trace reads for quiescent and reactivated NIH 3T3 cells(n=9 biological replicates). B') ECAR data for quiescent and reactivated cells compiled from multiple experiments(n=9 biological replicates). C) ECAR trace read comparing active and reactivated 3T3 cells(n=9 biological replicates). (Box and whisker plots= The box represents the upper/lower quartile of the data presented the line within the box is the mean of the data presented. The whisker represent the maximum and minimum of the data.) C') ECAR data for active and reactivated cells compiled from multiple experiments(n=9 biological replicates). D) NAD/NADH ratios for active and reactivated 3T3 cells (n=9 biological replicates). E) Protein measurements showing no difference in protein content in samples used in Seahorse mitochondrial assays(n=9 biological replicates). F) OCR measurements comparing quiescent and reactivated NIH 3T3 cells compiled from

multiple experiments(n=9). G) Energy map for quiescent and reactivated NIH 3T3 cells(n=9 biological replicates). H) OCR measurements for active NIH 3T3 cells or quiescent 3T3 cells(n=9 biological replicates).. Error bars represent 1X standard deviation *p<.05 **p<.005, calculated by students t-test

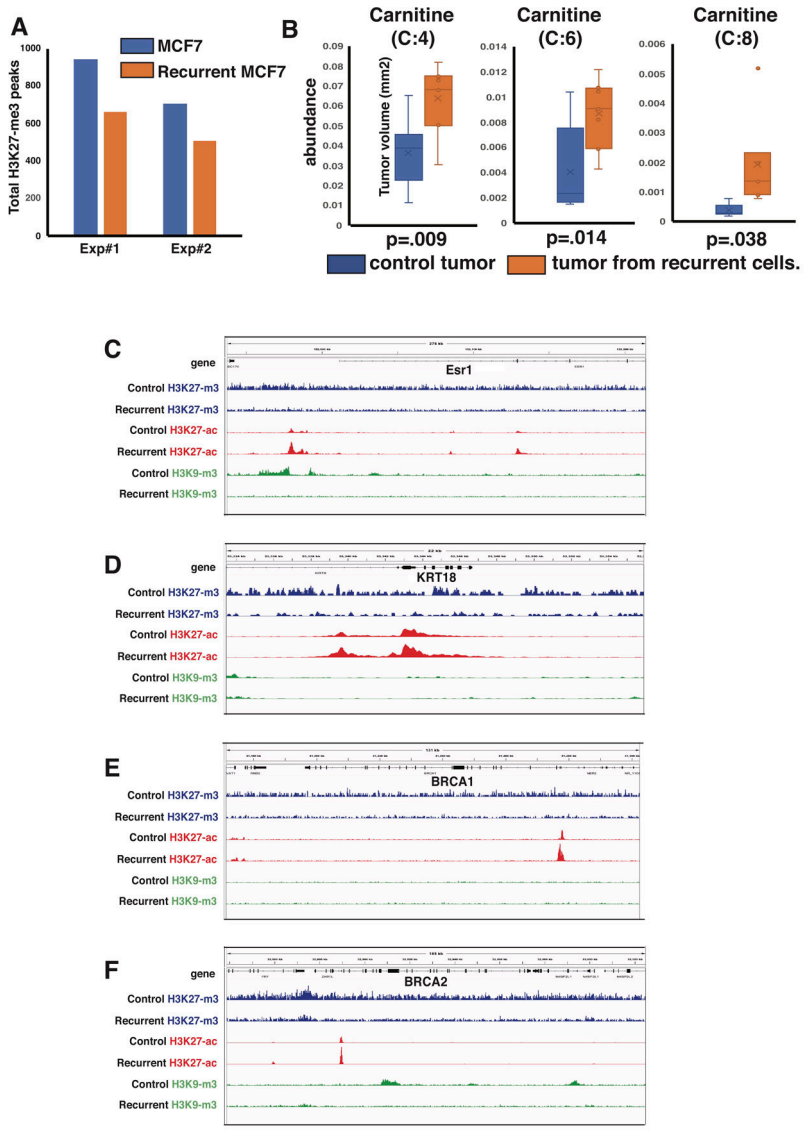

Extended Data Fig. 9. Chromatin changes in recurrent MCF7 cells.

A) Total number of broad methylation peaks in 2 independent ChIP-seq runs from control and recurrent MCF7 cells. B) LC/MS measurements of the levels of short-chain acyl-carnitines in control and recurrent MCF7 tumors (n=10 biological replicates) (Box and whisker plots= The box represents the upper/lower quartile of the data presented the line within the box is the mean of the data presented. The whisker represent the maximum and minimum of the data.). C)H3K27-me3, H3K27-ac, and H3K9-me3 ChIP seq profile of the genomic region that contains the 5'-end of Esr1 and its promoter. D) H3K27-me3, H3K27-ac, and H3K9-me3 ChIP seq profile of the genomic region that contains KRT18.

E) H3K27-me3, H3K27-ac, and H3K9-me3 ChIP seq profile of the genomic region that contains BRCA1. F) H3K27-me3, H3K27-ac, and H3K9-me3 ChIP seq profile of the genomic region that contains BRCA1.

Extended Data Table 1

Summary table of redox metabolism genes down-regulated in InR-DN expressing oocytes.

gene	logFC	PValue	FDR	Mat. Loaded	GO BIOLOGICAL PROCESS	Ortholog
Vha68-2	−1.041743	1.02E-06	2.44E-05	Y	ATP metabolic process	ATP6V1A
CG3321	−2.531166	0.000259	0.003009	Y	ATP synthesis coupled proton transport	ATP5ME
CG8177	−2.953726	3.75E-20	5.21E-18	Y	bicarbonate transport	SLC4A1
CG4860	−2.023663	1.19E-11	7.01E-10	Y	butyrate catabolic process	ACADS
AGBE	−1.459516	7.63E-10	3.44E-08	Y	carbohydrate metabolic process	GBE1
CG2938	−1.779595	3.50E-10	1.66E-08	Y	carbohydrate metabolic process	CASD1
CG10672	−2.109713	4.03E-12	2.52E-10	Y	carbonyl reductase (NADPH) activity	CBR3
CG8778	−2.097789	4.63E-09	1.84E-07	Y	fatty acid beta-oxidation	AUH
Mtpalpha	−1.635704	4.84E-11	2.68E-09	Y	fatty acid beta-oxidation	HADHA
Thiolase	−2.848269	1.22E-18	1.50E-16	Y	fatty acid beta-oxidation	HADHB
CG6543	−2.257908	3.29E-13	2.29E-11	Y	fatty acid beta-oxidation	ECHS1
yip2	−1.207071	5.25E-08	1.67E-06	Y	fatty acid beta-oxidation	ACAA2
CG4586	−3.905579	1.08E-52	3.20E-49	Y	fatty acid beta-oxidation	ACOX1
CG12512	−2.693354	2.00E-10	1.00E-08	Y	fatty acid biosynthetic process	ACSF2
CG5568	−2.74504	7.74E-09	2.96E-07	Y	fatty acid biosynthetic process	ACSBG1
Tpi	−1.073906	0.0018687	0.014812	Y	gluconeogenesis	TPi1
Gclc	−1.008345	2.55E-05	0.000414	Y	glutathione biosynthetic process	GCLC
CG10365	−1.057672	2.02E-05	0.000338	N	glutathione catabolic process	CHAC1
GstE3	−1.141332	3.20E-06	6.75E-05	N	glutathione metabolic process	GSTT1
GstT2	−1.146126	8.22E-05	0.001136	Y	glutathione metabolic process	GSTT2
GstE10	−3.382445	9.32E-11	4.93E-09	N	glutathione metabolic process	GSTT2B
GstT1	−1.880349	2.09E-19	2.75E-17	Y	glutathione metabolic process	GSTT2
CG9485	−1.026868	1.19E-07	3.49E-06	Y	glycogen biosynthetic process	AGL
GlyP	−2.871459	2.67E-30	9.70E-28	Y	glycogen catabolic process	PYGM
CG8475	−1.818253	2.74E-09	1.14E-07	Y	glycogen metabolic process	PHKB
Glycogenin	−1.513077	2.42E-12	1.54E-10	Y	glycogen metabolic process	GYG1
Hex-A	−1.811357	2.65E-19	3.45E-17	Y	glycolytic process	GCK
Pglym78	−1.187088	2.23E-07	6.24E-06	Y	glycolytic process	PGAM1
sima	−1.054028	4.98E-08	1.60E-06	Y	hypoxia repsonse	HIF1alpha
CG11334	−1.100718	8.09E-06	0.000151	Y	L-methionine salvage from methylthioadenosine	MRI1
CG5966	−2.81167	1.56E-12	1.02E-10	Y	lipid catabolic process	PNLIP
Tsc1	−1.239056	1.17E-09	5.16E-08	Y	lipid homeostasis	Tsc1

gene	logFC	PValue	FDR	Mat. Loaded	GO BIOLOGICAL PROCESS	Ortholog
Got1	−2.049305	1.53E-18	1.85E-16	Y	malate-aspartate shuttle	Got1
GC2	−1.930912	0.006232	0.037759	Y	malate-aspartate shuttle	GC2
aralar1	−1.996363	4.46E-22	7.44E-20	Y	malate-aspartate shuttle	SLC25A12
CG4365	−1.589969	2.00E-05	0.000336	Y	methylglyoxal catabolic process	HAGH
MCU	−2.42654	1.99E-16	2.05E-14	Y	mitochondrial calcium ion transmembrane transport	MCU
CG6463	−1.644186	0.001393	0.011778	Y	mitochondrial electron transport, NADH to ubiquinone	NDUFA3
CG32649	−1.715114	1.97E-13	1.38E-11	Y	mitochondrial electron transport, ubiquinol to cytochrome c	COQ8B
ATPsyn-d	−1.896013	0.000748	0.007175	Y	mitochondrial respiratory chain complex	ATP5PD
CG10320	−1.725896	0.006591	0.039323	Y	mitochondrial respiratory chain complex I assembly	NDUFB3
mRpL44	−1.408949	0.005367	0.033616	Y	mitochondrial translation	MRPL44
CG5010	−1.340264	0.005906	0.036164	Y	mitochondrion organization	CHCHD2
CG9940	−1.028282	3.63E-07	9.64E-06	Y	NAD biosynthetic process	NADSYN1
Mdh1	−1.884495	4.61E-09	1.83E-07	Y	NAD metabolic process	MDH1
Mdh2	−1.110017	9.75E-06	0.000179	Y	NAD metabolic process	MDH2
CG33156	−1.961921	2.00E-18	2.37E-16	Y	NAD metabolic process	NADK
Naam	−3.415207	1.61E-22	2.82E-20	Y	NAD metabolism	ISOC1
Gdh	−2.251665	2.72E-31	1.12E-28	Y	NADH oxidation	GLUD1
Idh	−1.180155	2.26E-06	4.94E-05	Y	NADP metabolic process	IDH1
CG2604	−1.031533	1.06E-05	0.00019	Y	oxidation-reduction process	SCCPDH
Cyp4d2	−1.029467	0.004887	0.031223	N	oxidation-reduction process	CYP4V2
Dhod	−1.133477	0.004139	0.027509	Y	oxidation-reduction process	DHODH
Aldh-III	−1.188816	4.52E-08	1.46E-06	Y	oxidation-reduction process	ALDH3B1
Alr	−1.098841	0.006636	0.039546	Y	oxidation-reduction process	GFER
CG10863	−2.6426	3.14E-21	4.71E-19	Y	oxidation-reduction process	AKR1B10
CG13822	−1.195139	4.23E-08	1.38E-06	Y	oxidation-reduction process	IFI30
CG18547	−1.205704	0.000665	0.006547	Y	oxidation-reduction process	AKR7A2
CG3397	−3.58479	6.76E-15	5.84E-13	N	oxidation-reduction process	AKR7A2
CG4174	−1.390725	1.05E-09	4.69E-08	y	oxidation-reduction process	P4HA3
CG6084	−2.958207	1.75E-27	4.91E-25	Y	oxidation-reduction process	AKR1B1
CG7277	−1.150095	0.001783	0.014256	Y	oxidation-reduction process	COQ6
CG7280	−1.64714	2.48E-06	5.38E-05	Y	oxidation-reduction process	SUOX
CG7737	−2.388972	7.34E-19	9.24E-17	Y	oxidation-reduction process	PAOX
CG8399	−1.218958	0.000244	0.002874	Y	oxidation-reduction process	FRRS1
CG9436	−1.269772	5.96E-06	0.000116	Y	oxidation-reduction process	AKR1B1
CG9674	−1.05342	5.29E-08	1.68E-06	N	oxidation-reduction process	none
CRYL1	−1.3711	0.002041	0.015895	N	oxidation-reduction process	CRYL1

gene	logFC	PValue	FDR	Mat. Loaded	GO BIOLOGICAL PROCESS	Ortholog
Cyp6a19	−1.713409	5.06E-05	0.000757	Y	oxidation-reduction process	CYP3A4
Cyp6a20	−2.131683	5.71E-08	1.80E-06	N	oxidation-reduction process	CYP3A4
Dhc36C	−1.182305	1.92E-05	0.000325	Y	oxidation-reduction process	DNAH7
Gapdh2	−1.119594	0.005557	0.034603	Y	oxidation-reduction process	GAPDH
Jafrac1	−1.34678	3.51E-07	9.39E-06	Y	oxidation-reduction process	PRDX2
Mgstl	−2.414145	1.19E-05	0.000212	Y	oxidation-reduction process	MGST1
Ppox	−2.0441	8.11E-17	8.61E-15	Y	oxidation-reduction process	PPOX
Prx3	−1.479543	0.000288	0.003309	Y	oxidation-reduction process	PRDX3
Pxn	−1.852767	5.85E-12	3.56E-10	N	oxidation-reduction process	PXDN
Sod2	−2.2132	8.68E-27	2.35E-24	Y	oxidation-reduction process	Sod2
Sptr	−1.115401	1.64E-06	3.70E-05	Y	oxidation-reduction process	SPR
Trxr-1	−1.406208	9.20E-06	0.00017	Y	oxidation-reduction process	TXNRD2
Cyp6v1	−2.426817	7.95E-26	1.97E-23	Y	oxidation-reduction process	CYP3A4
Pxt	−2.14198	3.81E-13	2.63E-11	Y	oxidation-reduction process	PXDN
Etf-QO	−1.534784	1.73E-09	7.40E-08	Y	oxidative phosphorylation / fatty acid beta-oxidation	ETFDH
Socs16D	−1.345714	1.85E-11	1.07E-09	Y	positive regulation of TORC1 signaling	SOCS7
Pdk	−2.103415	1.87E-22	3.20E-20	Y	pyruvate metabolic process	PDK3
CG2789	−1.042858	0.000302	0.003425	Y	regulation of oxidative phosphorylation	TSPO
CG14997	−1.265158	8.62E-07	2.09E-05	Y	sulfide oxidation, using sulfide:quinone oxidoreductase	SQOR
CG4095	−2.232898	0.001455	0.012165	N	tricarboxylic acid cycle	FH
Irp-1B	−2.928765	6.23E-20	8.57E-18	Y	tricarboxylic acid cycle	ACO1
Nc73EF	−1.027379	6.79E-08	2.12E-06	Y	tricarboxylic acid cycle	OGDH
dob	−2.63169	2.56E-26	6.66E-24	Y	triglyceride catabolic process	PNPLA2
CG17322	−3.02448	3.69E-32	1.68E-29	Y	xenobiotic metabolic process	UGT8

Supplementary Material

Refer to Web version on PubMed Central for supplementary material.

Acknowledgments

We thank B.H Graham, C.Thummel, and the Bloomington *Drosophila* stock center for reagents. We thank C.Thummel, M. Buszczak, R.Deberardinas, D.Hattori, J.Repa, and G. Demartino for providing insightful comments on the manuscript. Chao Xing and UTSW bioinformatics lab assisted with our sequencing data. We thank the U.T. Southwestern Animal resource core facility for their assistance with our xenograft studies. Ralph Deberardinas and the Children's Research Institute metabolomics core assisted with our LC/MS experiments. We also thank B. Tu and W.C. Hsieh for helpful discussions and ongoing technical support. All Model panels in this manuscript were made using Biorender.com (license number MJ22RADMPS). This work is support by the Welch Foundation (I-2015-20190330 M.S.), NIH (R01AG067604 M.S.), the W.W. Caruth Jr Foundation, and the U.T. Southwestern Endowed Scholars program.

References

1. Kaur JA comprehensive review on metabolic syndrome. Cardiol Res Pract2014, 943162, doi:10.1155/2014/943162 (2014). [PubMed: 24711954]
2. Lopez-Candales AMetabolic syndrome X: a comprehensive review of the pathophysiology and recommended therapy. J Med32, 283–300 (2001). [PubMed: 11958275]
3. Agnoli Cet al.Metabolic syndrome and breast cancer risk: a case-cohort study nested in a multicentre italian cohort. PLoS One10, e0128891, doi:10.1371/journal.pone.0128891 (2015). [PubMed: 26030767]
4. Buescher JLet al.Evidence for transgenerational metabolic programming in Drosophila. Dis Model Mech6, 1123–1132, doi:10.1242/dmm.011924 (2013). [PubMed: 23649823]
5. Rechavi Oet al.Starvation-induced transgenerational inheritance of small RNAs in C. elegans. Cell158, 277–287, doi:10.1016/j.cell.2014.06.020 (2014). [PubMed: 25018105]
6. Palu RAS, Praggastis SA & Thummel CS Parental obesity leads to metabolic changes in the F2 generation in Drosophila. Mol Metab 6, 631–639, doi:10.1016/j.molmet.2017.03.012 (2017). [PubMed: 28702320]
7. Meng Ret al.Early famine exposure and adult disease risk based on a 10-year prospective study of Chinese adults. Heart106, 213–220, doi:10.1136/heartjnl-2019-315750 (2020). [PubMed: 31704783]
8. Weiser NE & Kim JK Multigenerational Regulation of the Caenorhabditis elegans Chromatin Landscape by Germline Small RNAs. Annu Rev Genet 53, 289–311, doi:10.1146/annurev-genet-112618-043505 (2019). [PubMed: 31150586]
9. Ost Aet al.Paternal diet defines offspring chromatin state and intergenerational obesity. Cell159, 1352–1364, doi:10.1016/j.cell.2014.11.005 (2014). [PubMed: 25480298]
10. Gkountela Set al.DNA Demethylation Dynamics in the Human Prenatal Germline. Cell161, 1425–1436, doi:10.1016/j.cell.2015.05.012 (2015). [PubMed: 26004067]
11. Tang WWet al.A Unique Gene Regulatory Network Resets the Human Germline Epigenome for Development. Cell161, 1453–1467, doi:10.1016/j.cell.2015.04.053 (2015). [PubMed: 26046444]
12. Houtkooper RH, Pirinen E & Auwerx J Sirtuins as regulators of metabolism and healthspan. Nat Rev Mol Cell Biol 13, 225–238, doi:10.1038/nrm3293 (2012). [PubMed: 22395773]
13. Shi L & Tu BP Acetyl-CoA and the regulation of metabolism: mechanisms and consequences. Curr Opin Cell Biol 33, 125–131, doi:10.1016/j.ceb.2015.02.003 (2015). [PubMed: 25703630]
14. Sieber MH, Thomsen MB & Spradling AC Electron Transport Chain Remodeling by GSK3 during Oogenesis Connects Nutrient State to Reproduction. Cell 164, 420–432, doi:10.1016/j.cell.2015.12.020 (2016). [PubMed: 26824655]
15. Hsu HJ & Drummond-Barbosa D Insulin signals control the competence of the Drosophila female germline stem cell niche to respond to Notch ligands. Dev Biol 350, 290–300, doi:10.1016/j.ydbio.2010.11.032 (2011). [PubMed: 21145317]
16. Drummond-Barbosa D & Spradling AC Alpha-endosulfine, a potential regulator of insulin secretion, is required for adult tissue growth control in Drosophila. Dev Biol 266, 310–321 (2004). [PubMed: 14738879]
17. LaFever L & Drummond-Barbosa D Direct control of germline stem cell division and cyst growth by neural insulin in Drosophila. Science 309, 1071–1073, doi:10.1126/science.1111410 (2005). [PubMed: 16099985]
18. Kockel Let al.Dynamic switch of negative feedback regulation in Drosophila Akt-TOR signaling. PLoS Genet6, e1000990, doi:10.1371/journal.pgen.1000990 (2010). [PubMed: 20585550]
19. Anderson LKet al.Juxtaposition of C(2)M and the transverse filament protein C(3)G within the central region of Drosophila synaptonemal complex. Proc Natl Acad Sci U S A102, 4482–4487, doi:10.1073/pnas.0500172102 (2005). [PubMed: 15767569]
20. Hennig KM & Neufeld TP Inhibition of cellular growth and proliferation by dTOR overexpression in Drosophila. Genesis 34, 107–110, doi:10.1002/gene.10139 (2002). [PubMed: 12324961]

21. Petrova Bet al.Dynamic redox balance directs the oocyte-to-embryo transition via developmentally controlled reactive cysteine changes. Proc Natl Acad Sci U S A115, E7978–E7986, doi:10.1073/pnas.1807918115 (2018). [PubMed: 30082411]
22. Tennessen JMet al.Coordinated metabolic transitions during Drosophila embryogenesis and the onset of aerobic glycolysis. G3 (Bethesda)4, 839–850, doi:10.1534/g3.114.010652 (2014). [PubMed: 24622332]
23. Ni JQet al.Vector and parameters for targeted transgenic RNA interference in Drosophila melanogaster. Nat Methods5, 49–51, doi:10.1038/nmeth1146 (2008). [PubMed: 18084299]
24. Tennessen JM, Barry WE, Cox J & Thummel CS Methods for studying metabolism in Drosophila. Methods 68, 105–115, doi:10.1016/j.ymeth.2014.02.034 (2014). [PubMed: 24631891]
25. Contrino Set al.modMine: flexible access to modENCODE data. Nucleic Acids Res40, D1082–1088, doi:10.1093/nar/gkr921 (2012). [PubMed: 22080565]
26. Horner MAet al.The Drosophila DHR96 nuclear receptor binds cholesterol and regulates cholesterol homeostasis. Genes Dev23, 2711–2716, doi:10.1101/gad.1833609 (2009). [PubMed: 19952106]
27. Sieber MH & Thummel CS The DHR96 nuclear receptor controls triacylglycerol homeostasis in Drosophila. Cell Metab 10, 481–490, doi:10.1016/j.cmet.2009.10.010 (2009). [PubMed: 19945405]
28. Obniski R, Sieber M & Spradling AC Dietary Lipids Modulate Notch Signaling and Influence Adult Intestinal Development and Metabolism in Drosophila. Dev Cell 47, 98–111 e115, doi:10.1016/j.devcel.2018.08.013 (2018). [PubMed: 30220569]
29. Reuter Get al.Dependence of position-effect variegation in Drosophila on dose of a gene encoding an unusual zinc-finger protein. Nature344, 219–223, doi:10.1038/344219a0 (1990). [PubMed: 2107402]
30. Serefidou M, Venkatasubramani AV & Imhof A The Impact of One Carbon Metabolism on Histone Methylation. Front Genet 10, 764, doi:10.3389/fgene.2019.00764 (2019). [PubMed: 31555321]
31. Mitra M, Ho LD & Coller HA An In Vitro Model of Cellular Quiescence in Primary Human Dermal Fibroblasts. Methods Mol Biol 1686, 27–47, doi:10.1007/978-1-4939-7371-2_2 (2018). [PubMed: 29030810]
32. De Angelis ML, Francescangeli F, La Torre F & Zeuner A Stem Cell Plasticity and Dormancy in the Development of Cancer Therapy Resistance. Front Oncol 9, 626, doi:10.3389/fonc.2019.00626 (2019). [PubMed: 31355143]
33. Moore N & Lyle S Quiescent, slow-cycling stem cell populations in cancer: a review of the evidence and discussion of significance. J Oncol 2011, doi:10.1155/2011/396076 (2011).
34. Carone BRet al.Paternally induced transgenerational environmental reprogramming of metabolic gene expression in mammals. Cell143, 1084–1096, doi:10.1016/j.cell.2010.12.008 (2010). [PubMed: 21183072]
35. Sharma Uet al.Biogenesis and function of tRNA fragments during sperm maturation and fertilization in mammals. Science351, 391–396, doi:10.1126/science.aad6780 (2016). [PubMed: 26721685]
36. Bundgaard J & Barker JS Genetic variation for resistance to high temperature stress of mature sperm - a study in Drosophila. PLoS One 12, e0173990, doi:10.1371/journal.pone.0173990 (2017). [PubMed: 28358879]
37. Gao Jet al.Heat shock protein expression enhances heat tolerance of reptile embryos. Proc Biol Sci281, 20141135, doi:10.1098/rspb.2014.1135 (2014). [PubMed: 25080340]
38. Lockwood BL, Julick CR & Montooth KL Maternal loading of a small heat shock protein increases embryo thermal tolerance in Drosophila melanogaster. J Exp Biol 220, 4492–4501, doi:10.1242/jeb.164848 (2017). [PubMed: 29097593]
39. Thayer ZM, Wilson MA, Kim AW & Jaeggi AV Impact of prenatal stress on offspring glucocorticoid levels: A phylogenetic meta-analysis across 14 vertebrate species. Sci Rep 8, 4942, doi:10.1038/s41598-018-23169-w (2018). [PubMed: 29563562]
40. Leatherman JL & Jongens TA Transcriptional silencing and translational control: key features of early germline development. Bioessays 25, 326–335, doi:10.1002/bies.10247 (2003). [PubMed: 12655640]

41. Lovett JA & Goldstein ES The cytoplasmic distribution and characterization of poly(A)+RNA in oocytes and embryos of Drosophilia. Dev Biol 61, 70–78 (1977). [PubMed: 411706]

42. Mermod JJ, Jacobs-Lorena M & Crippa M Changes in rate of RNA synthesis and ribosomal gene number during oogenesis of Drosophila melanogaster. Dev Biol 57, 393–402 (1977). [PubMed: 406151]

43. Rossari F, Zucchinetti C, Buda G & Orciuolo E Tumor dormancy as an alternative step in the development of chemoresistance and metastasis - clinical implications. Cell Oncol (Dordr), doi:10.1007/s13402-019-00467-7 (2019).

44. Cao Det al.Inhibition of PGC-1alpha after chemotherapy-mediated insult confines multiple myeloma cell survival by affecting ROS accumulation. Oncol Rep33, 899–904, doi:10.3892/or.2014.3635 (2015). [PubMed: 25434963]

45. Mastropasqua F, Girolimetti G & Shoshan M PGC1alpha: Friend or Foe in Cancer? Genes (Basel) 9, doi:10.3390/genes9010048 (2018).

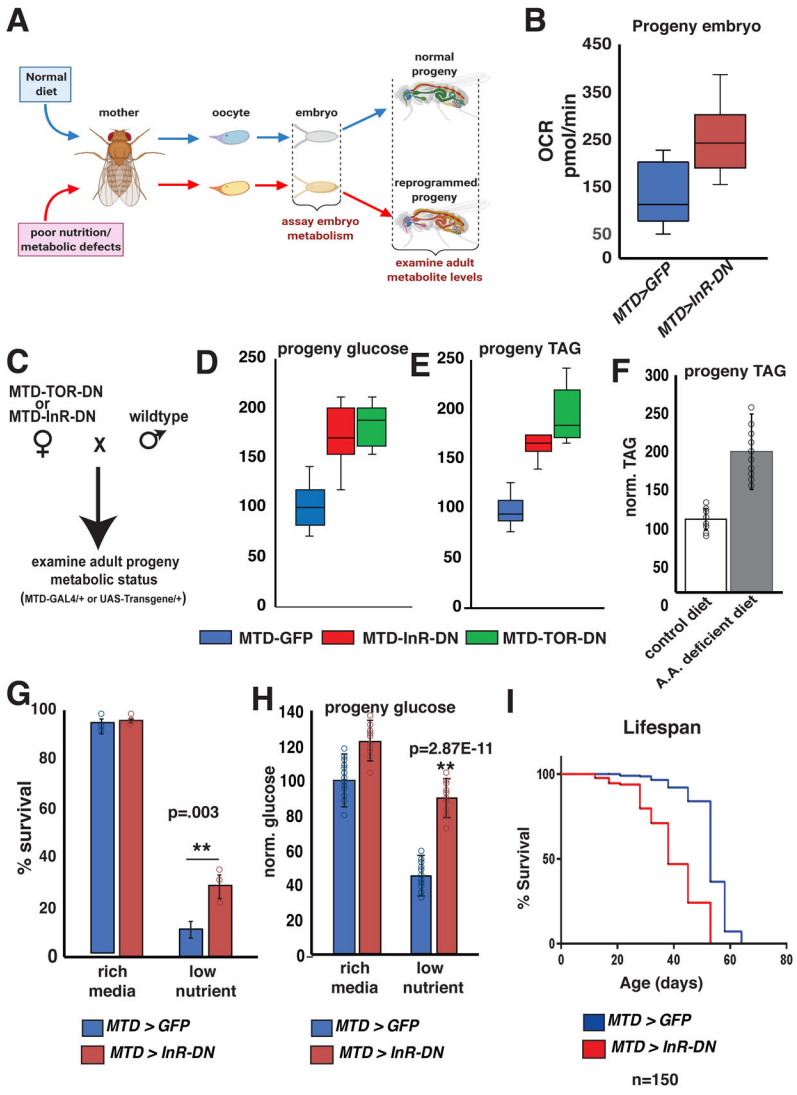

Figure 1. Inducing MRQ prematurely in oogenesis causes induced the reprogramming of progeny metabolism.

A) A diagram depicting the experimental strategy used to determine if changes in metabolism in the female germline induce the reprogramming of progeny metabolism. B) Oxygen consumption rate (OCR) measurements from MTD-GFP (control) embryos and embryonic progeny produced from MTD-InR-DN oocytes (n=9 independent biological replicates, p=0.003 calculated by students t-test) C) A scheme to determine if disrupting germline metabolism can induce lasting changes in progeny metabolism. D) Normalized glucose levels and triglyceride levels (E) of adult progeny produced from MTD-GFP, MTD-InR-DN, and MTD-TOR-DN oocytes (n= 12 independent biological replicates). The genotype of the progeny collected in these experiments are either *w; MTD-GAL4/+* or *w; UAS-transgene/+* F) TAG levels from the adult progeny of *Oregon R* mothers fed an amino acid-deficient diet (n=10 independent biological replicates). G) Measurements of progeny survival to adulthood on rich media and low nutrient media from control progeny and progeny produced from InR-DN expressing oocytes (n >1200 progeny). H)

Normalized glucose levels of adult progeny produced from MTD-GFP and MTD-InR-DN oocytes fed either a rich diet or a low-nutrient diet (n= 15 independent biological replicates). I) Longevity plot depicting the lifespan of progeny from MTD-GFP and MTD-InR-DN animals (n=150 progeny animals, $p<0.0001$, calculated by Mantel-Cox test). All glucose, glycogen, and triglyceride measurements are normalized to total protein. (Box and whisker plots= The box represents the upper/lower quartile of the data presented the line within the box is the mean of the data presented. The whisker represent the maximum and minimum of the data.) p values calculated by one-way anova. Error bars represent 1X standard deviation. *p<.05 **p<.005

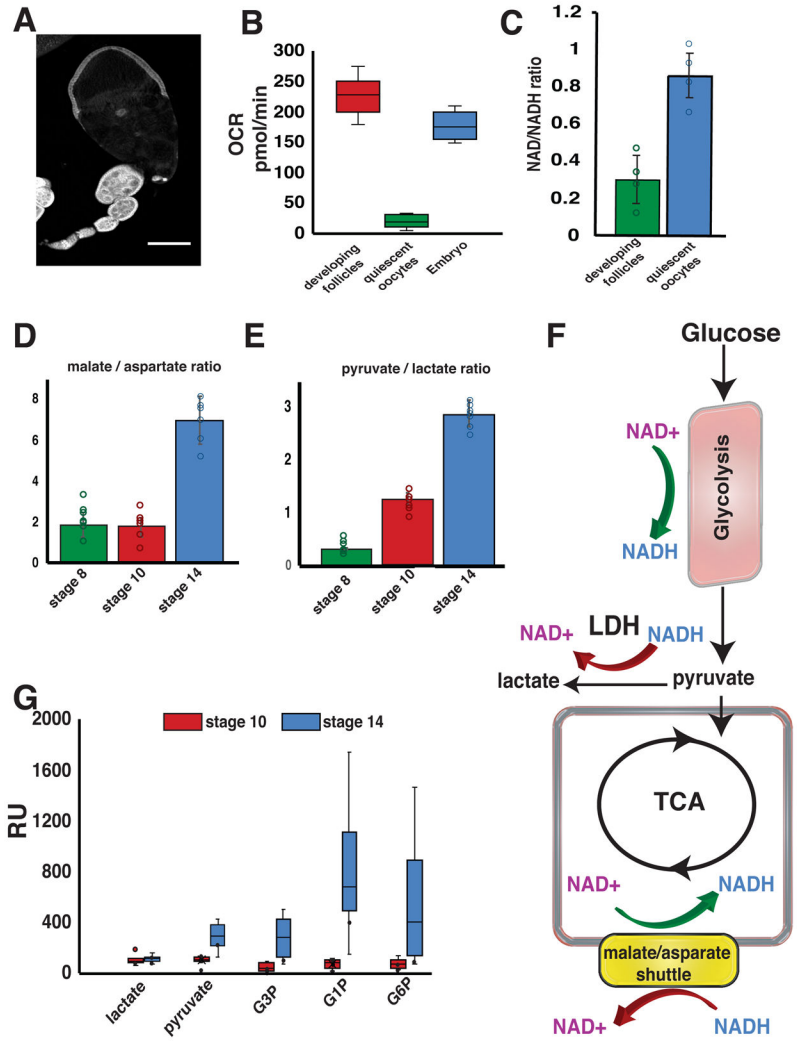

Figure 2. Oocytes establish a unique redox state during the onset of quiescence.

A) TMRE mitochondrial membrane potential staining of a wild-type ovariole (n=25 independent biological replicates) scale bar = 30μm. B) Oxygen consumption rate OCR measurements of early-stage follicles, mature oocytes, and embryos(n=9 independent biological replicates). These measurements are normalized to total protein. C) NAD^+/NADH ratios of early-stage follicles and mature oocytes (n=6 independent biological replicates, p=0.009, calculated by students t-test). Malate/aspartate (p=0.016) (D) and Pyruvate/lactate (p= 0.004) (E) ratios from control and InR-DN expressing oocytes (n=10 independent biological replicates, p values calculated by one-way anova) (Box and whisker plots= The box represents the upper/lower quartile of the data presented the line within the box is the mean of the data presented. The whisker represent the maximum and minimum of the data.). These data show that the major sources of NAD^+ regeneration are suppressed in quiescent oocytes. F) A model showing the major metabolic mechanisms that maintain NAD^+/NADH redox balance. G) GC/MS metabolomics data showing that glycolysis is suppressed in quiescent oocytes (p values calculated by one-way anova). All GC/MS-based

measurements in this figure contained n=10 biological replicates. Error bars represent 1X standard deviation

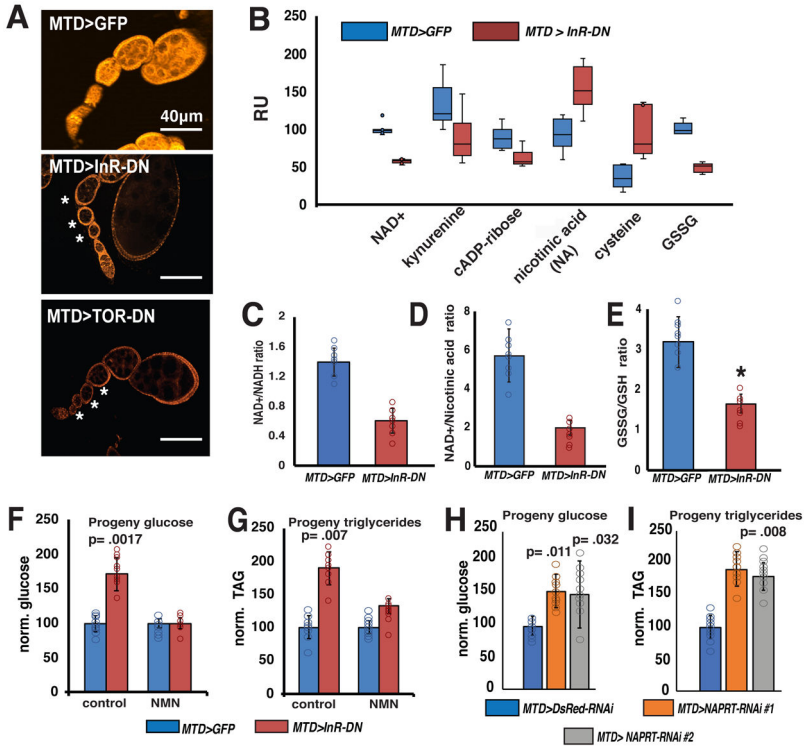

Figure 3. Changes in NAD metabolism are a heritable factor that drives the reprogramming of progeny metabolism.

A) Mitochondrial membrane potential staining of MTD-GFP, MTD-InR-DN, and MTD-TOR-DN expressing ovarioles. Asterisks show follicles where mitochondria are depolarized in early germ cells (n=25 biological replicates). B) LC/MS measurements of metabolites involved in NADH and GSH redox (n=8 biological replicates). (Box and whisker plots= The box represents the upper/lower quartile of the data presented. The line within the box is the mean of the data presented. The whisker represent the maximum and minimum of the data.) C) NAD^+/NADH ratios measurements of MTD-GFP and MTD-InR-DN oocytes (n=6 biological replicates, p=1.5E-5). D) NAD+/nicotinic acid ratios of MTD-GFP and MTD-InR-DN expressing oocytes (p=1.1E-4). E) GSSG/GSH ratios of MTD-GFP and MTD-InR-DN expressing oocytes(n=8 biological replicates) (p=0.014). F) Glucose and (G) triglyceride levels of control progeny and progeny produced from InR-DN expressing oocytes and how these levels are affected by maternal nicotinamide mononucleotide (NMN) supplementation(n=12 biological replicates, p-values calculated by one-way anova). Glucose (H) and triglyceride (I) levels of progeny from MTD-DsRed-RNAi and MTD-NAPRT-RNAi oocytes (n=12 biological replicates, p values calculated by one-way anova. Error bars represent 1X standard deviation

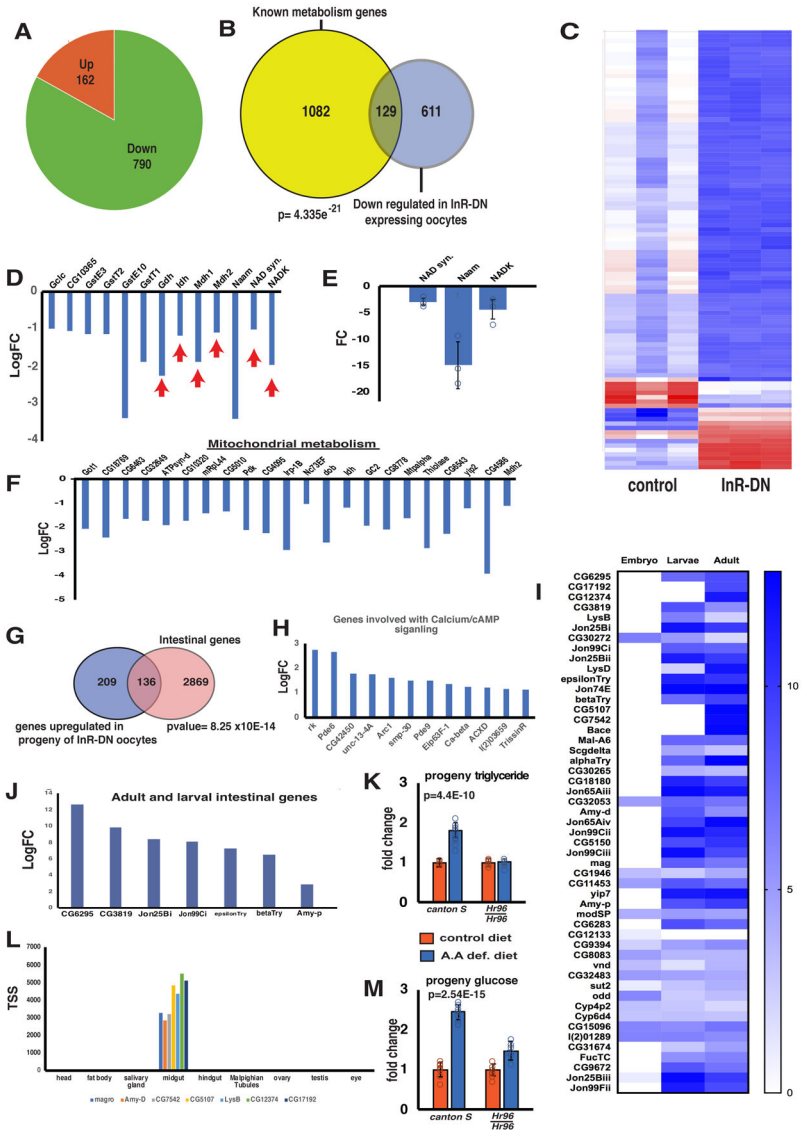

Figure 4. Inducing MRQ prematurely causes downregulation of redox metabolism genes and defective maternal RNA loading.

A) A pie chart that shows the relative distribution of significantly up-regulated and down-regulated genes in InR-DN expressing oocytes (FDR<.05). B) A Venn diagram showing the overlap between gene down-regulated in InR-DN expressing oocytes and a published list of Drosophila metabolism genes. Statistics reflect a fisher's exact test. C) A heatmap showing the top 100 miss-regulated genes in InR-DN expressing oocytes. D) Graph showing NADH and glutathione metabolism genes down-regulated in InR-DN expressing oocytes Red arrows highlight the genes directly involved with NAD regeneration and NAD+ biosynthesis. E) Q-PCR validation of the expression changes of enzymes directly involved with NAD metabolism(n=3 biological replicates). F) Graph showing several mitochondrial metabolism genes that are down-regulated in InR-DN oocytes. Fold changes in C, D, and F are expressed as log2 fold change. G) A Venn diagram and statistics showing the overlap between the genes up-regulated in the embryonic progeny of InR-DN expressing oocytes

and a previously characterized list of genes expressed in intestines. (p=8.25E-14) Statistics reflect a fisher's exact test. H) . Graph showing the top genes involved with calcium/cAMP signaling that are de-repressed in the embryonic progeny of InR-DN expressing oocytes. I) The developmental expression heatmap for the top 50 intestinal genes de-repressed the progeny of InR-DN expressing oocytes based on modEncode data. Data are presented as log2 expression of TSS normalized expression data. J) The developmental expression profile of 7 adult specific intestinal genes de-repressed in InR-DN progeny. Progeny triglyceride (K) and glucose (M) levels from control (Canton S) or *Hr96* mutants from parents fed either control or amino acid-deficient media. Measurements are presented as a fold change relative to the control diet (n=15 biological replicates). L) A graph depicting seven genes expressed in the adult and larval intestine that are up-regulated in the embryonic progeny of InR-DN expressing oocytes. All RNA-seq data presented is based on 3 independent biological replicates.

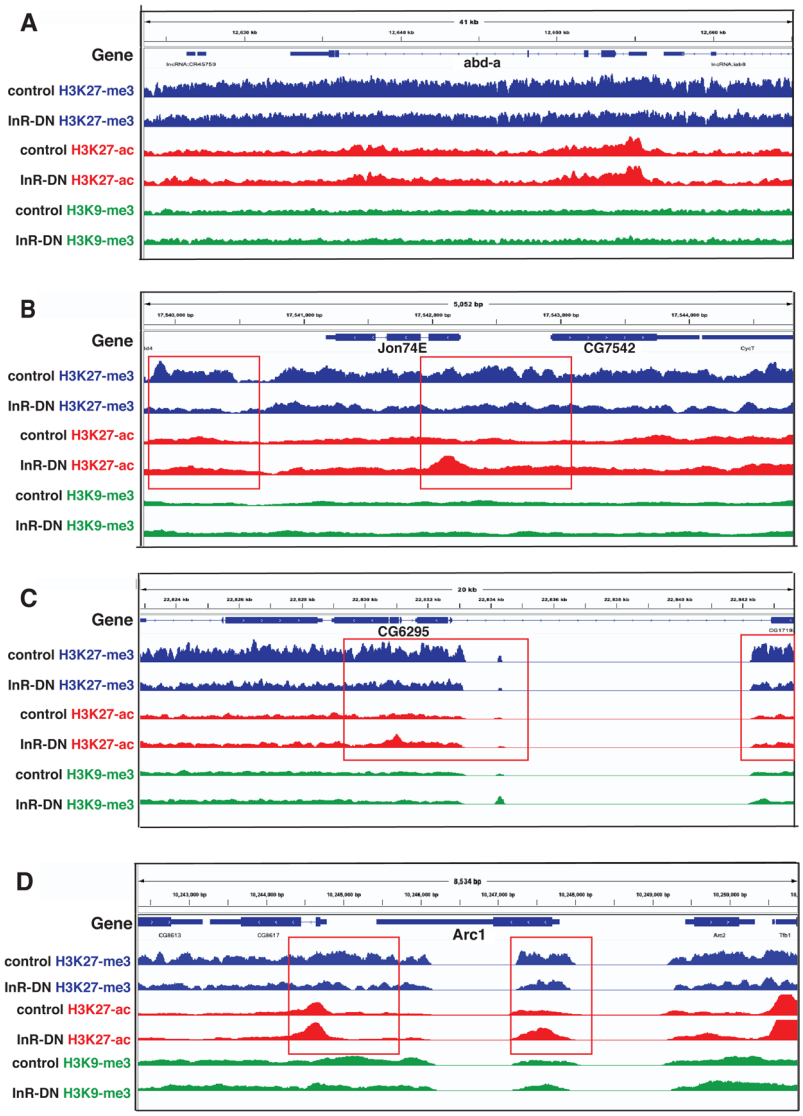

Figure 5. Reprogrammed progeny display lower levels of H3K27-me3

A) ChIP-seq profiles of the hox gene abd-a loci showing the levels of H3k27-me3, H3K27-ac, and H3K9-me3 in embryonic control progeny and progeny from InR-DN expressing oocytes. B) ChIP-seq profiles of the intestinal peptidase genes CG7542 and Jon74E loci showing the levels of H3k27-me3, H3K27-ac, and H3K9-me3 in embryonic control progeny and progeny from InR-DN expressing oocytes.

C) ChIP-seq profiles of the intestinal lipase CG6295 loci showing the levels of H3k27-me3, H3K27-ac, and H3K9-me3 in embryonic control progeny and progeny from InR-DN expressing oocytes.

D) ChIP-seq profiles of the calcium response gene ARC1 loci showing the levels of H3k27-me3, H3K27-ac, and H3K9-me3 in embryonic control progeny and progeny from InR-DN expressing oocytes. All ChIP-seq data presented is based on 2 independent biological replicates.

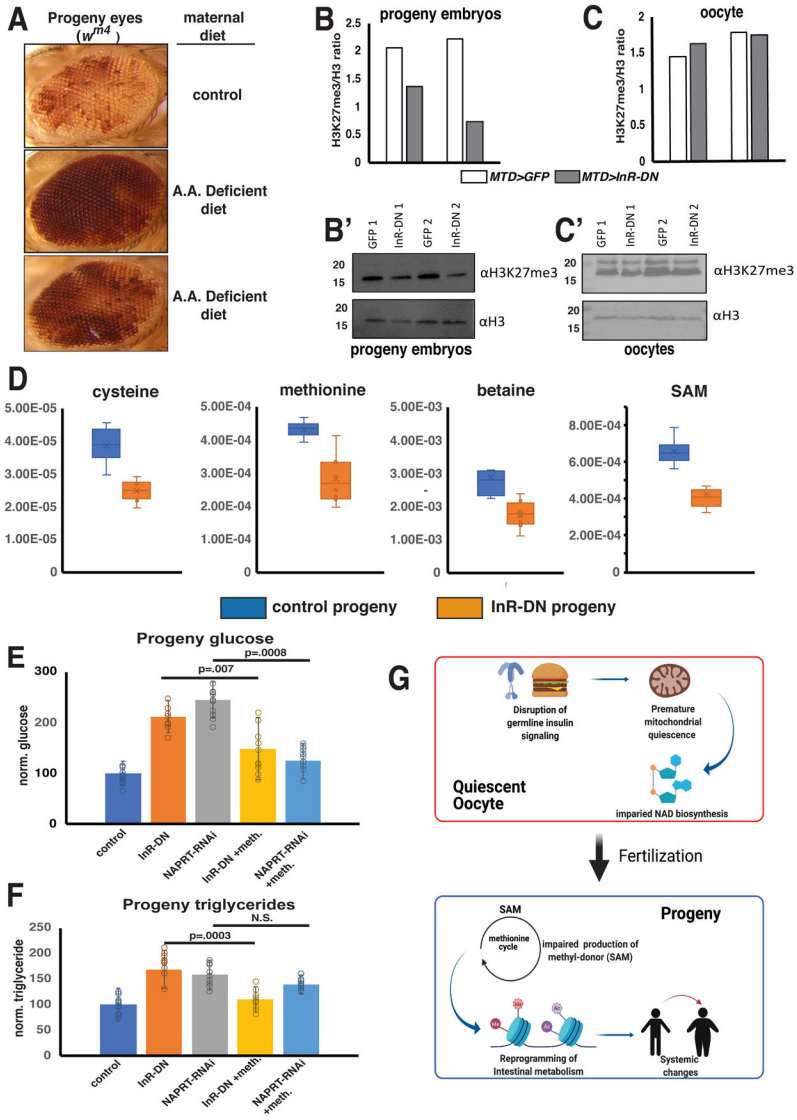

Figure 6. Defective methionine cycle activity underlies the loss of H3K27-me3 and contributes to the reprogramming of progeny metabolism.

A) Images showing W^{m4} variegation of progeny derived from mothers fed either a control diet or an amino acid-deficient diet. B,B')H3K27-me3/H3 ratios for control embryo and progeny embryos of InR-DN expressing oocytes from two independent replicate western blot experiments. C,C') H3K27-me3/H3 ratios for control oocytes and InR-DN expressing oocytes from two replicate western blot experiments. Source images in supplemental data. D) Levels of methionine cycle intermediates in control and InR-DN progeny measured by LC/MS. (Box and whisker plots= The box represents the upper/lower quartile of the data presented the line within the box is the mean of the data presented. The whiskers represent the maximum and minimum of the data. E) glucose levels from control, MTD-InR-DN, and MTD-NAPRT-RNAi progeny fed either a control diet or a methionine supplemented diet (n=10 biological replicates, p=0.007, p=0.0008 calculated by one-way anova). F) triglyceride levels from control, MTD-InR-DN, and MTD-NAPRT-RNAi progeny fed either a control diet or a methionine supplemented diet (n=12 biological replicates, p=0.0003

calculated by one way anova). G) A model of how redox metabolites, such as NAD and SAM, induce the reprogramming of progeny metabolic state in response to maternal metabolic stress. Error bars represent 1X standard deviation.

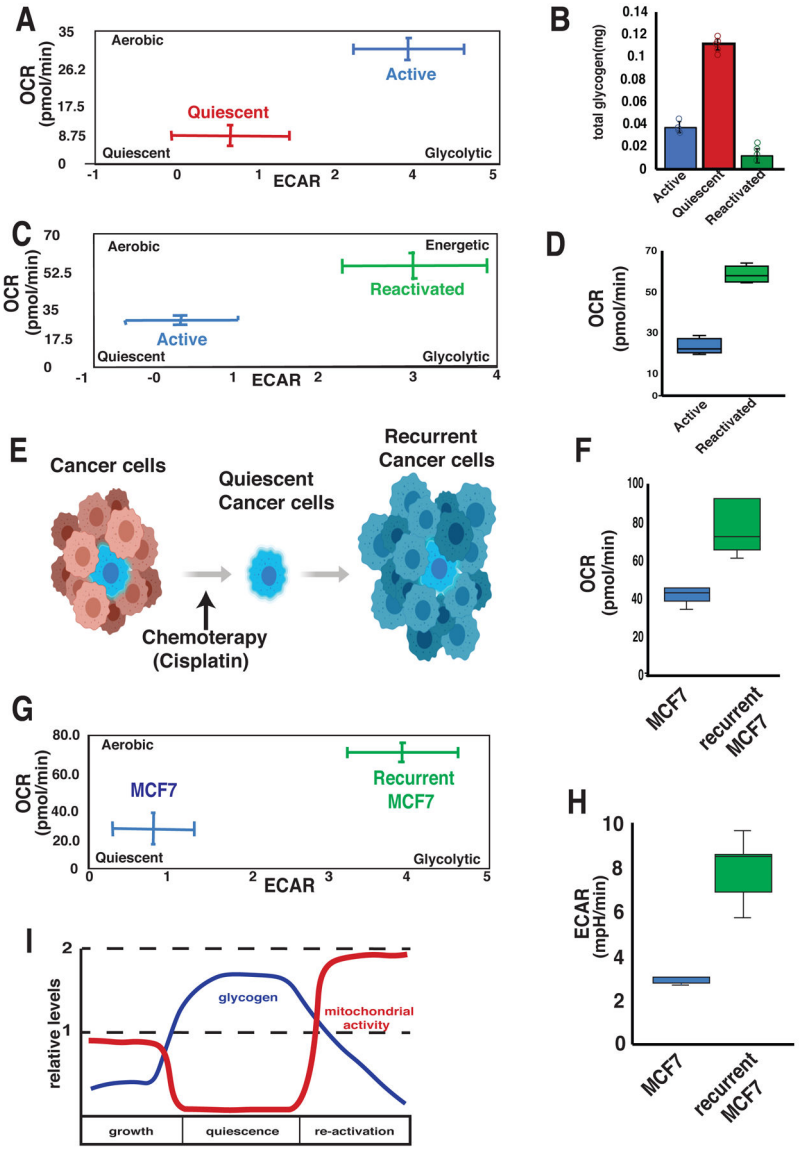

Figure 7. Quiescence has a conserved role in the reprogramming of progeny metabolism.

A) Oxygen consumption (OCR) is plotted against extracellular acidification rate (ECAR) for actively growing and quiescent NIH 3T3 cells (n=9). Glycogen levels (B) for active, quiescent, and reactivated 3T3 cells (n=6 biological replicates). C) Oxygen consumption (OCR) is plotted against extracellular acidification rate (ECAR) for active NIH 3T3 cells and NIH 3T3 cells that were quiescent for two days and then reactivated by increasing serum levels (n=12 biological replicates). D) Oxygen consumption (OCR) measurements were compiled from multiple experiments, comparing actively 3T3 cells to reactivated 3T3 cells (n=9 biological replicates). E) A model explaining the chemotherapy paradigm we used to determine if quiescence during chemotherapy treatment induces progeny metabolic reprogramming to support the aggressive regrowth of recurrent cancers. F) Oxygen consumption (OCR) measurements were compiled from multiple experiments comparing actively growing MCF7 cells to recurrent MCF7 cells (n=12 biological replicates). G) Oxygen consumption (OCR) is plotted against extracellular acidification rate (ECAR) for

growing MCF7 cells and recurrent MCF7 cells (n=12 biological replicates). H) ECAR measurements compiled from multiple experiments comparing actively growing MCF7 cells to recurrent MCF7 cells (n=12 biological replicates). I) a model depicting the changes in mitochondrial activity and glycogen storage observed as cell transition from growth, to quiescence and from quiescence to the reactivation of growth. Error bars represent 1X standard deviation. *p<.05 **p<.005

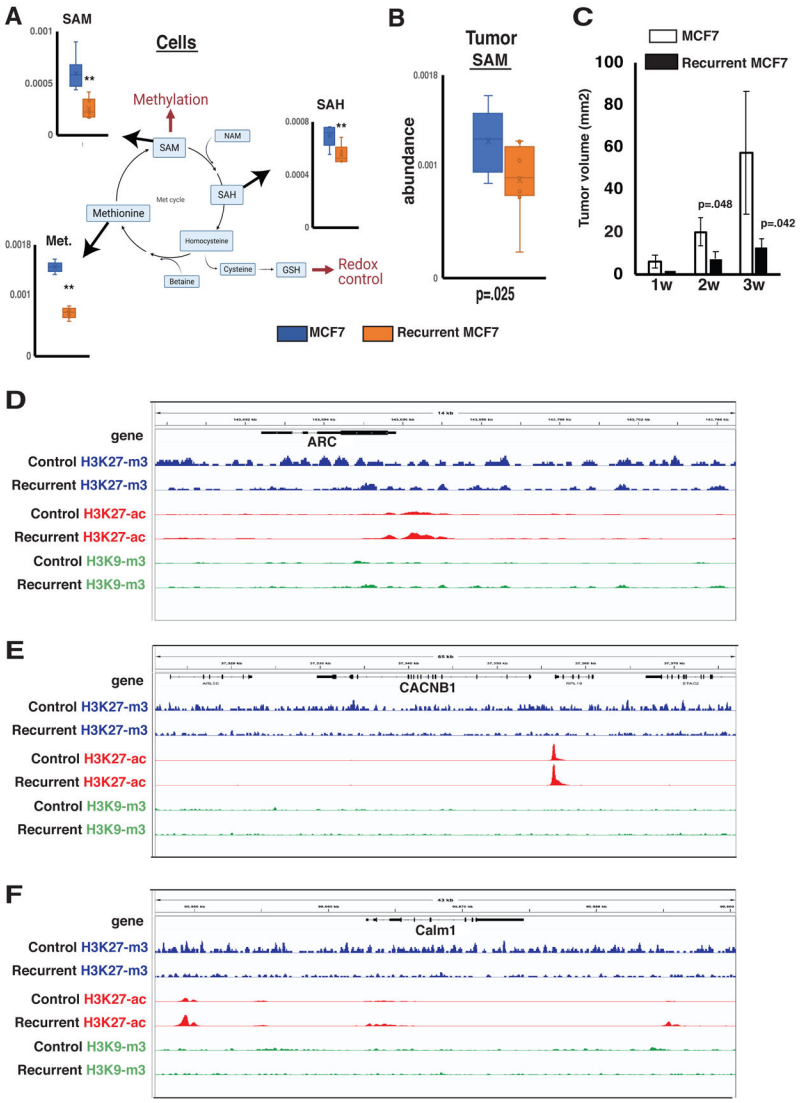

Figure 8. A Mammalian model of progeny metabolic reprogramming displays reduced levels of H3K27-me3.

1) LC/MS-based measurements of methionine cycle intermediates Methionine, SAH, and SAM in MCF& cells and recurrent MCF7 cells(n=8 biological replicates). B) SAM levels in control and recurrent MCF7 xenograft tumors (n=8 biological replicates). (Box and whisker plots= The box represents the upper/lower quartile of the data presented the line within the box is the mean of the data presented. The whisker represent the maximum and minimum of the data.) C) Xenograft tumor growth rate data from control MCF7 cells and recurrent MCF7 cells(n=16 biological replicates) D) H3K27-me3, H3K27-ac, and H3K9-me3 ChIP seq profile of the genomic region that contains the calcium response gene ARC. E) H3K27-me3, H3K27-ac, and H3K9-me3 ChIP seq profile of the genomic region that the calcium channel subunit CACNB1. F) H3K27-me3, H3K27-ac, and H3K9-me3 ChIP seq profile of the genomic region that contains calmodulin 1 (CALM1). All ChIP-seq data presented is based on 2 independent biological replicates. Error bars represent 1X standard deviation.